

TANSPEC: TIFR-ARIES Near Infrared Spectrometer

Saurabh Sharma^{a*}, Devendra K. Ojha^b, Arpan Ghosh^a, Joe P. Ninan^b, Supriyo Ghosh^b, Swarna K. Ghosh^b, P. Manoj^b, Milind B. Naik^b, Savio L. A. D’Costa^b, B. Krishna Reddy^a, Nandish Nanjappa^a, Rakesh Pandey^a, Tirthendu Sinha^a, Neelam Panwar^a, Susmitha Antony^{b,c}, Harmeen Kaur^d, Sanjit Sahu^a, Tarun Bangia^a, Satheesha S. Poojary^b, Rajesh B. Jadhav^b, Shailesh B. Bhagat^b, Ganesh S. Meshram^b, Harshit Shah^b, John T. Rayner^e, Douglas W. Toomey^f, and Pradeep R. Sandimani^b

^a Aryabhata Research Institute of Observational Sciences (ARIES), Manora Peak, Nainital 263 001, India

^b Tata Institute of Fundamental Research (TIFR), Homi Bhabha Road, Colaba, Mumbai - 400 005, India

^c Indian Institute of Astrophysics (IIA), II Block, Koramangala, Bengaluru 560 034, India

^d Center of Advanced Study, Department of Physics DSB Campus, Kumaun University Nainital, 263001, India

^e Institute for Astronomy, University of Hawaii, 2680 Woodlawn Drive, Honolulu, HI 96822, USA

^f Mauna Kea Infrared, LLC, 21 Pookela St. Hilo, HI 96720, USA

E-mail: saurabh@aries.res.in

March 2022

Abstract. We present the design and performance of the TANSPEC, a medium-resolution $0.55 - 2.5 \mu\text{m}$ cryogenic spectrometer and imager, now in operation at the 3.6-m Devasthal Optical Telescope (DOT), Nainital, India. The TANSPEC provides three modes of operation which include, photometry with broad- and narrow-band filters, spectroscopy with short slits of $20''$ length and different widths (from $0.5''$ to $4.0''$) in cross-dispersed mode at a resolving power R of ~ 2750 , and spectroscopy with long slits of $60''$ length and different widths (from $0.5''$ to $4.0''$) in prism mode at a resolving power R of $\sim 100\text{--}350$. TANSPEC’s imager mode provides a field of view of $60'' \times 60''$ with a plate scale of $0.245''/\text{pixel}$ on the 3.6-m DOT. The TANSPEC was successfully commissioned during April-May 2019 and the subsequent characterization and astronomical observations are presented here. The TANSPEC has been made available to the worldwide astronomical community for science observations from October 2020.

Keywords: Spectrometer, optics, infrared, imager

1. Introduction

An instrument with simultaneous optical and near-infrared (NIR) spectroscopic/imaging capabilities on a 4-m class telescope will be an ideal observational tool needed for the efficient usage of the telescope time and can act as a work-horse for numerous science cases. Recently, Aryabhata Research Institute of Observational Sciences (ARIES)[†], Nainital, India has installed a modern 3.6-m new technology optical telescope (3.6-m Devasthal Optical Telescope - DOT[‡]), the largest in India, at Devasthal (latitude = 29°21'39".4 N, longitude= 79°41'03".6 E, altitude = 2450 m), Nainital in Uttarakhand. This facility is a major national observing facility in India and therefore it is of great advantage to complement this telescope with an instrument having simultaneous optical-NIR coverage.

The TIFR-ARIES Near Infrared Spectrometer (TANSPEC) is built in collaboration with Tata Institute of Fundamental Research (TIFR)[§], Mumbai, India; ARIES, Nainital, India and Mauna Kea Infrared LLC (MKIR)[¶], Hawaii, USA for the 3.6-m DOT. It is a unique spectrograph which provides simultaneous wavelength coverage from $\sim 0.55 \mu\text{m}$ to $2.5 \mu\text{m}$ in spectroscopic (cross-dispersed (XD) mode with $R \sim 2750$ and prism mode with $R \sim 100-350$) as well as in imaging ($r'i'YJHK_s$ bands) modes. The importance of simultaneous optical-NIR observations has been realized in recent years for the Galactic and extragalactic astrophysical problems. The TANSPEC will be extremely sensitive to low temperature stellar photospheres ($T \sim 2500 \text{ K}$) and objects surrounded by warm dust envelopes or embedded in the dust/molecular clouds. It is therefore particularly suited to the study of low and very low mass stellar populations (M/L dwarfs, brown dwarfs), strong mass-losing stars on the asymptotic giant branch (AGB), young stellar objects (YSOs) still in their proto-stellar envelopes, Gravitational lenses, active galactic nuclei, etc. This instrument will also be ideal to produce a spectral library of a large number of stars which can be used as training samples for the future automated stellar classification tools. XD spectroscopy at resolving powers of $R \sim 2750$ ($\sim 110 \text{ km/s}$) with very broad spectral coverage (optical to NIR wavelengths) is very well suited to identify atomic and molecular features as well as to trace the high-speed dynamics such as stellar winds and broad-lined quasars. Deeply embedded YSOs and molecular species in protostellar disks, comets, and AGB stars are best observed at $\sim 2-2.5 \mu\text{m}$. The low-resolution prism mode is optimum for faint object spectroscopy such as brown dwarf spectral energy distribution, and solid-state features in asteroids and satellites. The long-slit in this mode is also useful to study extended objects such as planets and nebulae.

At present, all the existing 2-m class telescopes within India (viz. 2.01-m Himalayan *Chandra* Telescope^{||} at Hanle, Ladakh; 2-m Inter-University Center for Astronomy

[†]<https://aries.res.in/>

[‡]<https://aries.res.in/facilities/astrophysical-telescopes/360cm-telescope>

[§]<https://www.tifr.res.in>

[¶]<http://mkir.com/>

^{||}<https://www.iap.res.in/?q=iap.htm>

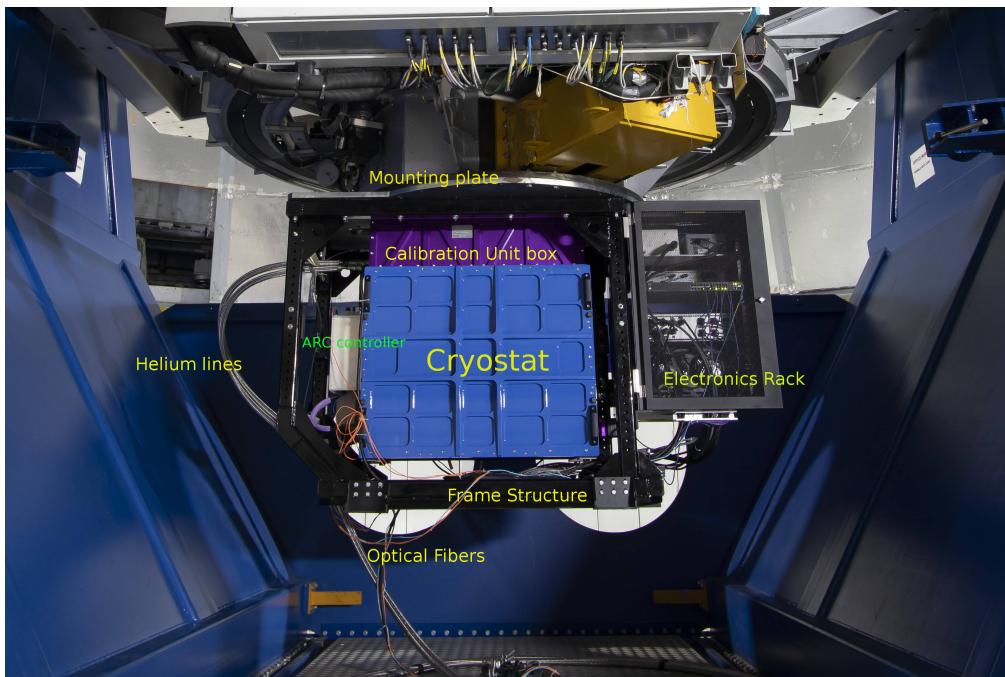


Figure 1. The TANSPEC mounted on the Cassegrain focus of the 3.6-m DOT. Various sub-components such as mounting plate, calibration unit box, cryostat, electronics rack, Helium lines, frame structure, and optical fibers of the TANSPEC instrument are also shown. The approximate size of this instrument (including electronic rack and mounting frame) is 2200 mm (length) x 1100 mm (width) x 1350 mm (height). The total weight of this instrument is 2000 kg, out of which, the instrument (blue+purple box) is 650 kg and mounting plate is of 350 kg. Remaining 1000 kg is added to the mounting frame to maintain the center of gravity to balance the telescope.

and Astrophysics telescope** near Pune; 2.34-m Indian Institute of Astrophysics telescope†† at Kavalur) have either optical or NIR imager/spectrograph instruments. The TANSPEC is only instrument in India and one of the few instruments around the globe with simultaneous optical-NIR capabilities. In this paper, we provide the details of the TANSPEC in Section 2 (Overview), Section 3 (Optics), Section 4 (Cryostat), Section 5 (Electronics and Control system), and Section 6 (Software). The details on detectors and their performance are presented in Section 7. The characterization and performances analyses of the TANSPEC instrument on the 3.6-m DOT are presented in Section 8 and we conclude in Section 9.

2. Instrument overview

A photograph of the TANSPEC mounted on the main port (Cassegrain focus) of the 3.6-m DOT through a rigid mounting plate is shown in Fig 1. The cryostat (blue box) is interfaced with a rigid box (purple), which houses a spectral calibration unit

**<http://www.iucaa.in/igo.html>

††<https://www.iiap.res.in/?q=vbo.htm>

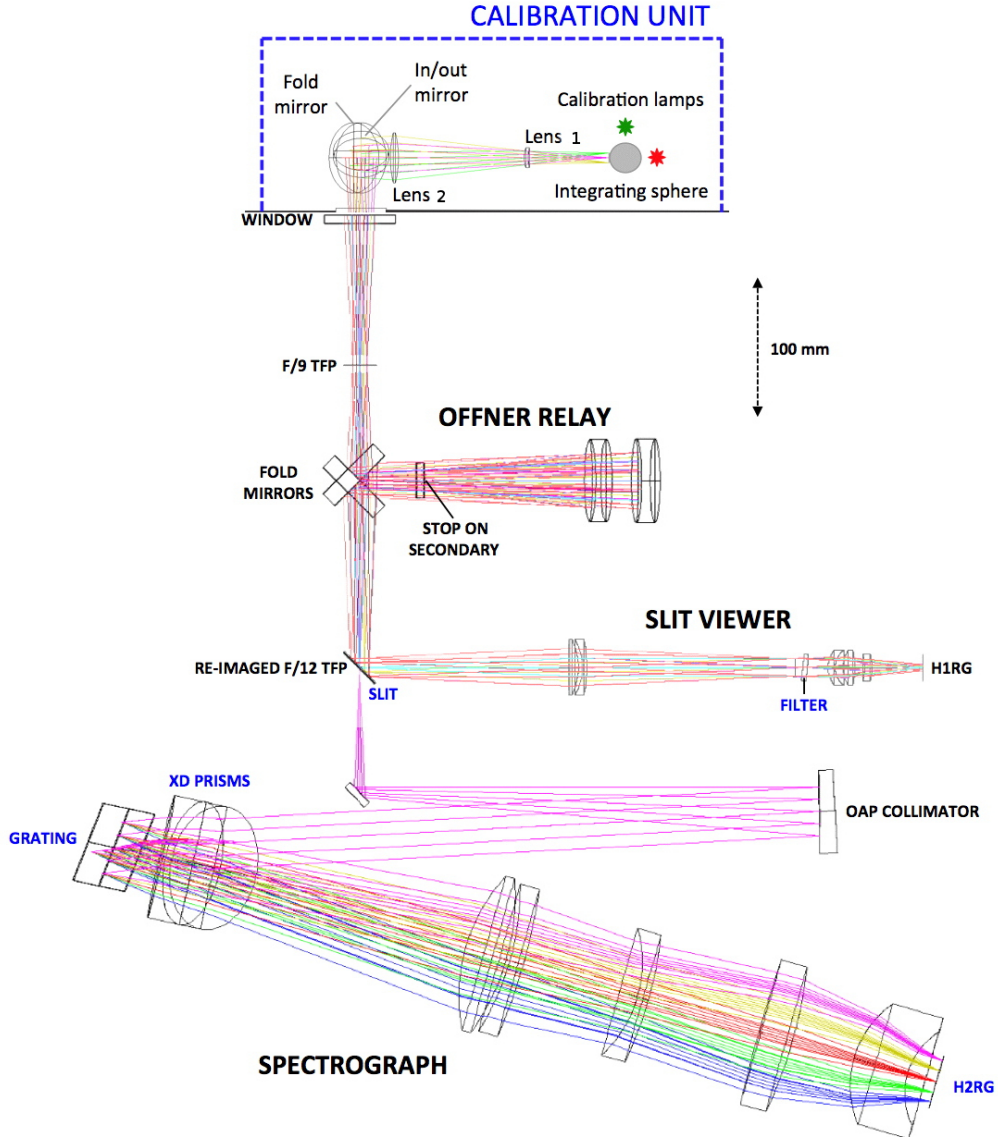


Figure 2. Overall optical layout of the TANSPEC comprising four major components: Calibration unit, fore-optics (Offner relay), slit viewer and spectrograph. The $f/9$ beam from the telescope comes to a focus at the telescope focal plane just inside the cryostat window. A $60 \times 60 \text{ arcsec}^2$ field of view is reimaged by an Offner relay onto the slit where it is reflected into the slit viewer and re-imaged onto an H1RG array at 0.25 arcsec per pixel. A slot in the slit transmits the $f/12$ beam into the spectrograph where it is dispersed and re-imaged onto an H2RG array. In this view ray tracing for order three in the cross-dispersed mode is shown. A warm calibration unit is located above the cryostat window.

consisting of transfer optics, integrating sphere, continuum and arc lamps and interfaces with the mounting plate of the instrument. The black frame in the photograph is the structure attached to the mounting plate which holds the counter-weights to balance this instrument and the electronics rack (black box). The electronics rack holds the power supplies, Ethernet power switches, temperature controller of the instrument. The photograph also shows the pair of Helium lines coming out from the instrument and going through the azimuth axis of the telescope to the ground floor of the telescope building and then to the closed-cycle cryo cooler's compressor. The optical fibers (orange cables) from the array controllers are going out to the located at the telescope observing room.

There are three sections which make up the cold optics inside the cryostat: the fore-optics, the infrared (IR) slit viewer/guider, and the spectrograph. The initial concept of this instrument is drawn from the SpeX [1], a medium-resolution $0.8\text{--}5.5\ \mu\text{m}$ spectrograph and imager for the NASA Infrared Telescope Facility (IRTF)^{††} at Hawaii. An overall view of the TANSPEC optical layout is shown in Fig 2. Briefly, the f/9 beam from the telescope or calibration lamp comes to a focus at the telescope focal plane (TFP) about 100 mm inside the CaF₂ window. The TFP is then reimaged at f/12 onto slits in the slit wheel by an Offner relay containing two concave mirrors and one convex secondary mirror. The slit mirrors are tilted at 45 degrees to the incoming f/12 beam and reflect it to the slit viewer for imaging and guiding using 1024×1024 pixels HAWAII-1RG (H1RG) array. The f/12 beam entering the spectrograph through the slot in the slit is first folded and then collimated on to a dispersing optics. The dispersed beam is focused onto a 2048×2048 pixels HAWAII-2RG (H2RG) array by a set of camera lenses. All the lenses are anti-reflection coated for $0.55\text{--}2.5\ \mu\text{m}$ wavelength range. This was a challenge because the wavelength range is broad and encompasses the visible and NIR range. We were able to achieve designs that gave around 2% reflectivity or less over the full wavelength range. As a typical visible wavelength filters are designed for CCDs with a $\sim 1\ \mu\text{m}$ wavelength cutoff, the filter used in the slit-viewer are specially designed to block out of band wavelengths upto $2.7\ \mu\text{m}$. This is required also because there is much higher background flux levels at the $1\text{--}2.5\ \mu\text{m}$ range. Individual Astronomical Research Cameras (ARC) array controllers run each of the spectrograph and imaging arrays and are mounted on the cryostat. The array controller uses a single-board SPARC computer and four digital signal processor (DSP) boards. A graphical user interface (GUI) of the TANSPEC runs on a Linux workstation placed in the observing room connected to the controllers of the arrays by the optical fibers.

^{††}<http://irtfweb.ifa.hawaii.edu/>

3. Optics

3.1. Calibration Unit

A calibration unit is used for the flat fielding and the wavelength calibration of the raw spectra taken through this spectrograph. As shown in Fig 2, it has an assembly of calibration lamps, integrating sphere, camera lenses, and a fold mirror (mounted on a linear translation stage that moves into the telescope beam and picks off the beam from the calibration lamps when required). The pick-off mirror and lamp control can be remotely operated from the instrument software. The calibration optics are designed in a way to match the telescope's f/number and to evenly illuminate the TFP inside the TANSPEC with a 15 mm diameter flat field. This is the size required to cover the longest slits (60 arcsec). A 12.5 mm diameter exit port (field stop) of an integrating sphere serves as the uniform (Lambertian) flat field. This field is magnified to 15 mm diameter by a 246 mm focal length lens (Lens 1) placed 82 mm from the exit port. A 125 mm focal length CaF₂ lens (Lens 2) re-images this field at 1:1 onto the f/9 TFP inside the cryostat. At the same time, Lens 2 images the 15 mm aperture stop of the Lens 1 onto the telescope secondary mirror to create an exit pupil identical to that of the telescope so that the calibration light sources illuminate the instrument identically to the telescope. The root mean square (RMS) spot diameter in the TFP from the calibration optics is about 0.5 mm. This is sufficient enough to satisfy the uniformity requirement of better than 1% across the slits, which is limited by the integrating sphere. The calibration unit has Argon and Neon Discharge lamps§§ and two Tungsten continuum (of different brightness) lamps which cover the entire wavelength range (0.55-2.5 μ m) of the spectrograph.

3.2. Fore Optics

The function of the fore-optics is to re-image the TFP onto the slits with the necessary magnification required for the spectrograph. At the same time an image of the entrance pupil needs to be formed where a cold stop can be located to baffle thermal flux and off-axis scattered light from the telescope. An optimized cold stop cannot be located in the spectrograph since the slit diffractively blurs the entrance pupil image. In the TANSPEC, this is achieved with an Offner relay (cf. Fig 3), which consists of three on-axis spherical mirrors. The primary and secondary of the offner relay consists of two concave and one convex mirrors, respectively. The two mirrors of the primary are a little different in focal length so that we can convert from f/9 beam to f/12 beam which is the desired F-number of the beam at the slit entrance to the spectrograph optics. This results in a slight reduction of the Offner optical performance that is not significant for the system performance. The Offner-relay is shown in Fig 3 with the folding flat mirrors removed. It re-images the f/9 60'' \times 60'' TFP onto the slit plane at f/12. We painted the center of the cold secondary of Offner relay (onto which telescope pupil is imaged) black

§§<https://www.newport.com/f/pencil-style-calibration-lamps>

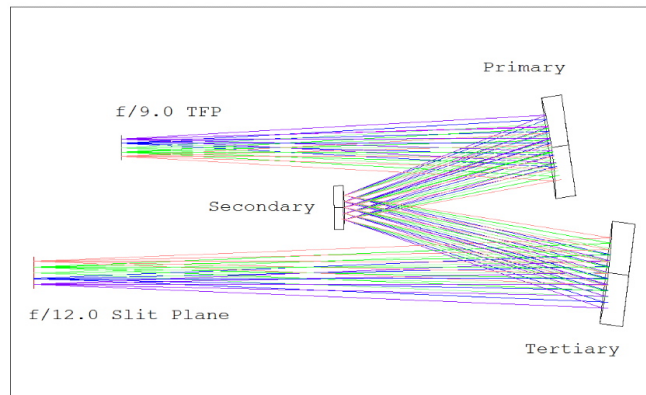


Figure 3. The fore-optics re-image the TFP onto the slit plane. This is done with an Offner relay. In this view the fold mirrors are removed and the slit plane is shown untilted. The telescope pupil of 14.3 mm diameter is imaged onto the Offner secondary mirror. A cold stop is placed here.

to work as a cold stop. Being all reflecting, the Offner relay is completely achromatic and has high and constant throughput across the desired wavelength range.

3.3. Slit viewer

The IR slit viewer allows spectra of very red and embedded objects through NIR guiding. It is also a fairly capable imager. The slit viewer is a collimator-camera re-imaging system consisting of BaF₂-LiF collimator and LiF-BaF₂-ZnSe camera lenses that re-image the 60'' × 60'' slit plane onto H1RG array with an image scale of $\sim 0.25''$ (cf. Fig 2). For Nyquist sampling of the field of view (FOV) reflected of the slit, only the central 480 × 416 pixel² area (starting from x=416 and y=288 pixels) is used. The collimator doublet forms another image of the system entrance pupil where slit-viewing filters are placed (each 25.4 mm diameter). This second stop is not optimized to cold baffle since the cold stop in the fore-optics does this. However, it is the best location for the imaging filters (small and uniform pupil image). The slit viewer has a filter-wheel with 12 slots to accommodate filters of different wavelengths. This wheel have position accuracy of 50 μ m. The details of the filters-wheel and filters used in the TANSPEC slit-viewer are given in Table 1 and Table 2, respectively. The Y, J, H, K_s filters are in Mauna Kea Observatory (MKO) system [2] make by Asahi Spectra, Japan. The r', i', H_2 , and $Br\gamma$ filters are made by Andover Corporation, USA***, where the r', i' filters are in the Sloan digital sky survey (SDSS) system [3]. The response curves for all the filters are provided in Fig 4.

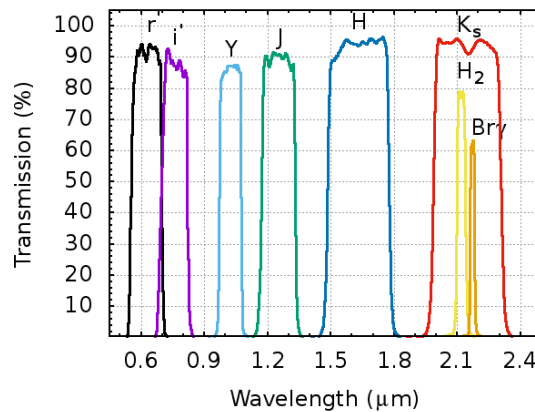
¶¶<https://www.asahi-spectra.com/>
 ***<https://www.andovercorp.com/>

Table 1. The details of the filter and slit wheels.

Position	Filter wheel		Slit wheel		
	Filter	Note	Slit width (")	Slit length (")	Note
1	J	Broad-band filter	0.5	20	XD mode
2	H	Broad-band filter	0.75	20	XD mode
3	K_s	Broad-band filter	1.0	20	XD mode
4	Y	Broad-band filter	1.5	20	XD mode
5	i'	Broad-band filter	2.0	20	XD mode
6	r'	Broad-band filter	4.0	20	XD mode
7	$Br\gamma$	Narrow-band filter	0.5	60	Prism mode
8	H_2	Narrow-band filter	1.0	60	Prism mode
9	Blank1	-	2.0	60	Prism mode
10	Blank2	-	4.0	60	Prism mode
11	Free slot	-	Mirror	-	Imaging mode
12	Pupil	-	Pupil	-	-

Table 2. Specification of the filters used in the slit-viewer of TANSPEC.

Filter Name	Central Wavelength (μm)	Wavelength range ^a (μm)	Photometric system
r'	0.612	0.555-0.670	SDSS
i'	0.744	0.681-0.805	SDSS
Y	1.020	0.970-1.070	MKO
J	1.250	1.170-1.330	MKO
H	1.635	1.490-1.780	MKO
K_s	2.150	1.990-2.310	MKO
H_2	2.122	2.097-2.138	-
$Br\gamma$	2.171	2.160-2.181	-

^a: at 50% transmission of the peak**Figure 4.** Response curves for the filters used in the slitviewer of TANSPEC.

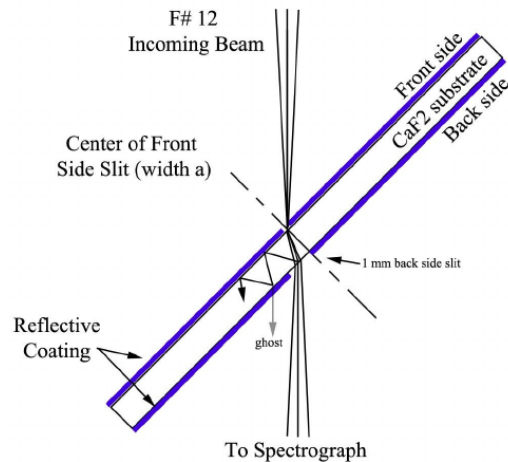


Figure 5. Description of a slit used in the TANSPEC instrument.

3.4. Spectrograph Unit

3.4.1. Slits The spectrograph unit has a slit-wheel with 12 slots to accommodate slits of different sizes and have a position accuracy of $50 \mu\text{m}$. The details of the slits are listed in Table 1 and is shown in Fig 5. The slits are 1.00 mm thick Fused Silica substrates that have a silver-coated mirror with a slot lithographically applied to the front surface. The slit mirror is oriented at 45 degrees to the incoming f/12 beam and reflects a $60 \times 60 \text{ arcsec}^2$ FOV into the slit viewer. Since the slit is applied lithographically, it is very sharp and any scatter from the slit edges is minimized. To avoid the ghost reflection at the back surface of the slit substrate entering the spectrograph, an absorbing surface is applied to the back surface of the slit substrate. This back surface has a suitably positioned slot to transmit the primary beam and absorb the ghost. The slit mirrors were coated with Aluminium and were made by Photosciences Inc, USA† † †.

3.4.2. XD mode The f/12 beam entering the spectrograph at the slit is first folded and then collimated by an Aluminium off-axis-parabolic (OAP) mirror. The OAP and its coatings were done by Durham University, Precision optics lab, UK‡ ‡ ‡. An image of the entrance pupil (35 mm diameter) is formed at a distance of one focal length from the OAP (420 mm). Grating and prism dispersing elements are located here, housed in the grating wheel. One position of the wheel houses the grating and cross-dispersing double prisms (the XD mode), and the other houses a mirror and single prism (the low-resolution mode). The dispersed beam is focused onto H2RG array by a five-element refractive camera lens: BaF2-ZnS-LiF-ZnSe-ZnSe. The optical layout and spectral format of the XD mode are shown in Fig 6. This mode is optimized for wavelengths $0.63\text{-}2.54 \mu\text{m}$ (orders 3-10). To minimize aberrations, these orders are

† † † <https://www.photo-sciences.com>

‡ ‡ ‡ <https://dpo.webspace.durham.ac.uk/>

Table 3. TANSPEC near-Litrow configuration in the XD mode.

Parameter	Value
R	2750
Slit width	0.5 arcsec (2 pixel sampling)
Slit length	20 arcsec in XD mode
Collimated beam diameter	35.0 mm
Grating blaze angle	17.5 degrees
Grating groove frequency	90 lines/mm
Grating blaze wavelength (m=1)	6.7 micron
Angle between incident and diffracted beams	9.5 degrees
ZnSe prism apex angle	15 degrees
FS prism apex angle	25 degrees
Input beam	f/12
OAP focal length	420 mm
OAP off-axis angle	5.5 degrees
Camera focal length	144 mm

centered on the array and the geometric (untoleranced) resolving power is $R \sim 2750$ at the center of each order. The H2RG array is sensitive from $0.4 \mu\text{m}$ to $2.5 \mu\text{m}$ approximately, therefore wavelengths $0.63 - 0.55 \mu\text{m}$ (orders 11-10) are also imaged onto the array but at slightly reduced resolution due to higher optical aberrations and minor vignetting in the camera lenses.

The configuration for the XD mode of the TANSPEC is given in Table 3. The grating used in the TANSPEC is an off-the-shelf master grating (Aluminium substrate) made by Richardson Gratings, USA, §§§ closely approximating the derived design. Fused Silica and ZnSe prisms are used in double-pass to achieve cross dispersion over the desired spectral range of $\sim 0.55\text{-}2.5 \mu\text{m}$. The prisms are vacuum spaced. There is a slight angle introduced into the second prism so that the two inner surfaces are at an angle to each other. This prevents fringing caused by the two surfaces being parallel. One disadvantage of prisms is that they usually have lower dispersion than gratings. Using the prisms in double pass configuration helps to compensate for this. Also, by using prisms made from Fused Silica and ZnSe the order separation can be made almost constant in wavelength over the range $\sim 0.55\text{-}2.5 \mu\text{m}$ leading to a much better use of the detector format than is possible for a single prism or grating (order separation is proportional to λ^2).

3.4.3. Prism mode In the prism mode, the grating and double prism are replaced by a mirror and single prism (cf. Fig 7). The prism is made of fused silica and is of size similar to the cross-dispersing prisms. The prisms and coatings on the prisms were

§§§<https://www.newport.com/b/richardson-gratings>

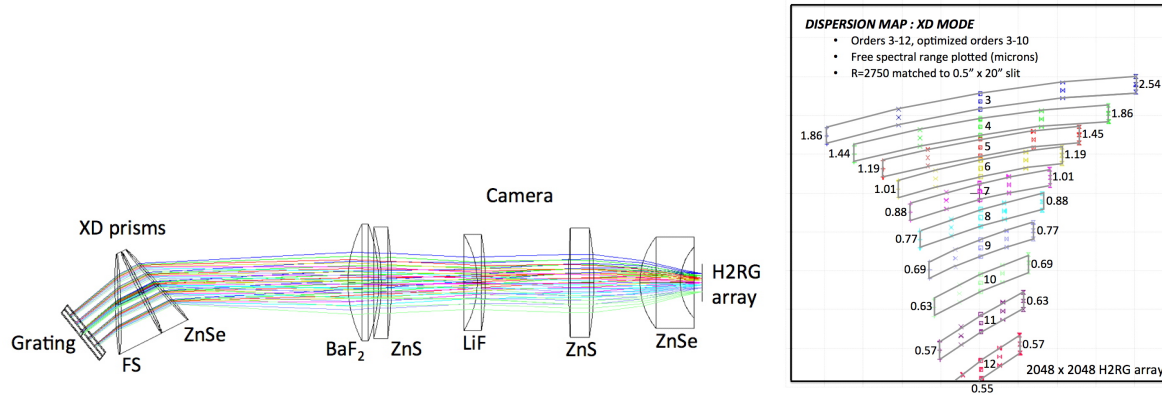


Figure 6. Left panel: Ray diagram of the spectrograph XD mode for orders 3-10. Right panel: Dispersion map in the XD mode optimized for 2.5-0.63 μm (orders 3-10). Orders 11-12 are covered but optical aberrations limit $R < 2500$. The H2RG array is sensitive between ~ 2.5 -0.4 μm .

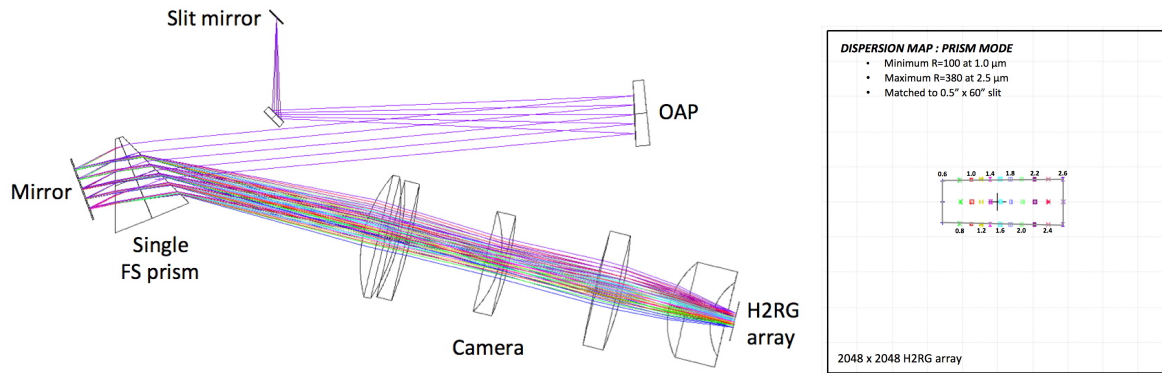


Figure 7. Left panel: Ray diagram for the prism (low-resolution) mode. Right panel: Dispersion map covering 0.55 - 2.5 μm wavelength range in the prism mode.

done by Rainbow Research Optics INC^{☞☞☞}. The dispersing elements are mounted in a grating wheel. All the other optics are unchanged. Consequently, stray light levels in the prism mode are very similar to those in the XD mode. The apex of the single Fused Silica prism is oriented at 90 degrees to apex of the double prisms of the XD mode so that dispersion is along array rows (in the XD mode, dispersion is along array columns). The resulting dispersion map is also shown in Fig 7. Due to the change in refractive index of Fused Silica with wavelength, R changes by a factor of three across the wavelength range. The prism is designed for $R \sim 100$ matched to the narrowest slit (0.5") at about 1.0 μm and is higher at shorter and longer wavelengths. A complication of the design is that the angle required to prevent the input and exit beams to the prism from colliding, creates anamorphic shrinking in the dispersion direction. This results in the low-resolution mode 0.5" slit being sampled by around three pixels instead of two pixels as in the XD mode (where the anamorphic effects are in the XD direction).

3.4.4. Stray Light and Baffling A cold Lyot stop in the fore-optics is used to control the thermal background and stray light from the telescope and sky. The light paths in the instrument are enclosed mostly in baffled tubes in Aluminium enclosures. The enclosures are designed in a way to prevent thermal background and stray light from the cryostat components which are warmer than ~ 80 K (e.g., drive shafts, wires, warm vacuum jacket etc.) that might scatter along the path of the light towards the detectors. The aim of the design was to keep instrument background below the dark current of the detector (~ 0.1 electron/sec). Because of the broad wavelength coverage of the TANSPEC, large variation in either sky or object brightness can occur across the spectra. Therefore, any ghost reflection from the brighter part of the spectrum to the fainter parts can degrade the quality of the data. The main areas of the concern are narcissus ghosts from the prisms and camera lens. The ray-tracing of the former suggests that these ghosts can be minimized by tilting the H2RG array by 1 degree (this is enough to redirect any ghost reflections off the prisms and incurring no measurable defocus across the array). The latter are extremely out of focus and it does not pose any concern. The amount of ghosting in the TANSPEC is of the order of few percent and can be removed by sky subtraction.

4. Cryostat

4.1. Mechanical structure

The entire mechanical assembly of the TANSPEC is shown in Fig 8. The TANSPEC instrument has an envelope size of 1900 mm (width) x 915 mm (length) x 1148 mm (height) which is within the telescope instrument envelop. The weight of the TANSPEC and its mounting plate are 650 kg and 350 kg, respectively. Therefore, to balance this instrument and maintain the center-of-gravity of the 3.6-m DOT, an extra frame with counterweights (1000 kg) on it is added to the instrument. Electronics cabinet containing power-supplies,

Lakeshore, USA temperature controller* and Western Telematic Inc. (WTI), USA Ethernet power switches† are also mounted on this frame. The TANSPEC is attached to the telescope through a mounting plate via a rigid interface box. This box is mounted in between the top plate and the vacuum jacket. A calibration unit is placed inside this box. The box is 280 mm deep and the walls are of 25 mm thickness. The top plate of the vacuum jacket contains the liquid nitrogen fill port, entrance window, and the mount for closed-cycle cooler. The TANSPEC along with its frame mounted on the 3.6-m DOT is shown in Fig 1.

The vacuum jacket of the TANSPEC has a four-sided center section weighing about 205 kg and is bolted by two large O-ring sealed covers, each weighing about 38 kg. The four-sided center section is made from four plates of 6061-T6-Aluminium which

*<https://www.lakeshore.com/products/categories/overview/temperature-products/cryogenic-temperature-controllers/model-336-cryogenic-temperature-controller>

†<https://www.wti.com/collections/power-transfer-switch>

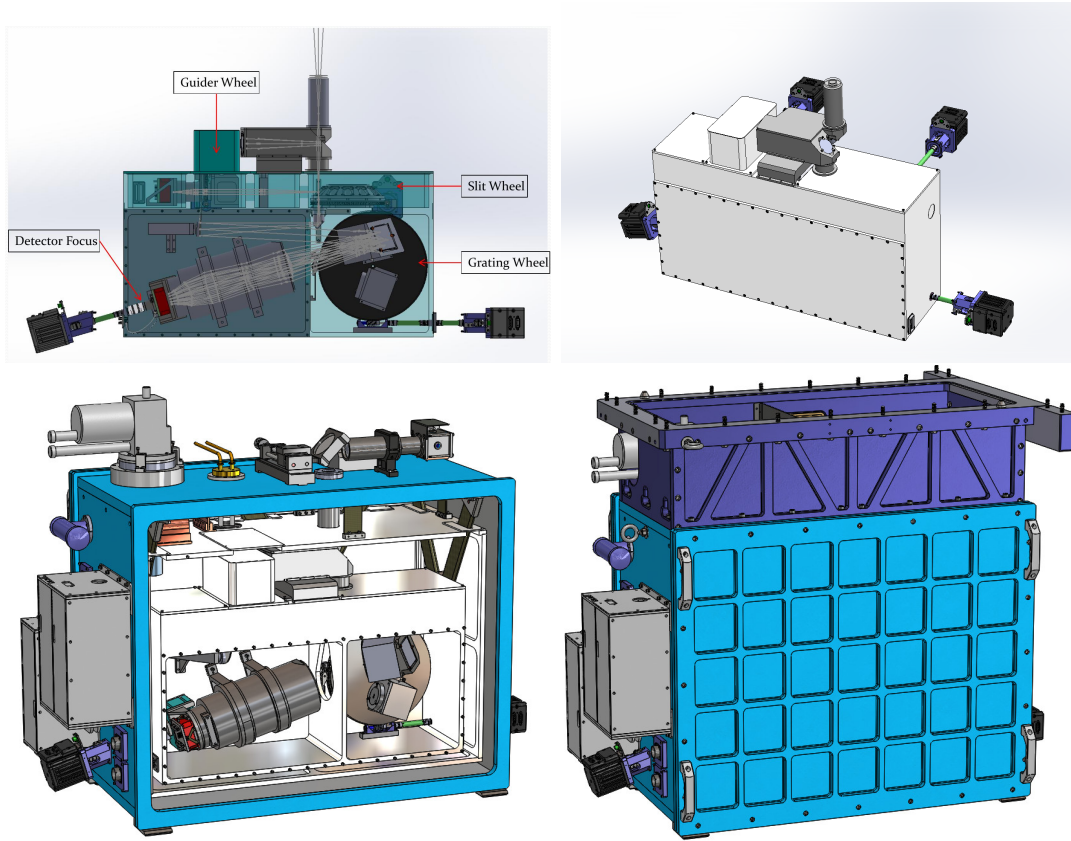


Figure 8. Mechanical assembly of the TANSPEC. The various mechanisms along with ray trace (top left), cold structure (top right), vacuum jacket (blue box), radiation shield, cold structure along with other components (bottom left), and the entire cryostat assembly (bottom right) along with top box (purple box containing calibration unit, LN₂ fill port, cold head) are shown.

are electron-beam welded together. The vacuum jacket has a external dimensions of 1070 mm (length) x 860 mm (height) x 630 mm (width). The vacuum jacket has no hard connections except at the rigid top plate (25 mm thick). Therefore, if we can keep the flexures below the yield strength of the Aluminium along with the flexure of shafts (connected to the warm motors mounted outside of the vacuum jacket) within the specifications, we can achieve a very stable configuration by using a thick vacuum jacket walls of 25.4 mm. Although, the large vacuum jacket covers are with ribs that taper up to 70 mm. All the internal surfaces are mirror finished to provide good radiation shielding and to improve the liquid Nitrogen (LN₂) hold time. Inside this there is an radiation shield which is closed-cycle cooler cooled shield that removes most of the thermal radiation from the vacuum jacket. The wall of the LN₂ cooled cold bench/box is 12.5 mm thick and hangs inside the vacuum jacket through fiber-glass V-trusses (3) which are connected to the top plate inside the radiation shield. The detectors are thermally clamped to the cold structure. The radiation shield is mounted around cold structure through four shear webs connected to the top of the vacuum jacket.

4.2. Mechanisms

The TANSPEC has mechanisms for the slit wheel, guide channel filter wheel, grating wheel, spectrograph channel detector focus and calibration unit pick-off mirror. It uses external warm smart motors manufactured by Animatics Corporation, USA.[‡] mounted on one of the two covers of the vacuum jacket and are coupled to the wheels through ferrofluidic vacuum feed-throughs. The optics and detectors can be accessed by unbolting the opposite covers. There is no need to disassemble motors for majority of the troubleshooting inside the cryostat. The array controllers are mounted on the outer surface of the cryostat. The mechanisms have three different categories, i.e., continuously variable wheels, discrete position wheels with detents, and a linear flex stage. For the position sensing, we have used the non-contact Hall effect devices similar to the SpeX instrument [4]. All the wheels are equipped with a stationary Hall effect sensor. These sensors are used to encode wheels position by placing the magnets at their edges. Opposite polarities signifies the homing and other positions. The Hall effect sensors outputs are passed through the comparator circuits and function like limit switches. Stepper motors of 400 steps/revolution in the worm-gear mechanisms is used to drive all the wheels with detented positions and the final position is determined by counting the steps taken from the home position. The H2RG array focus stage consists of an Aluminium alloy flex stage with anti-backlash linear position mechanism which provides ± 2.5 mm of focus travel through a screw coupled with a stepper motor. The calibration lamp assembly has a plane mirror which can be moved by using an motor and linear stage arrangement.

4.3. Cryogenic design and performance

The required cooling of this instrument is achieved through a hybrid system with closed-cycle cooling for the radiation shields and LN₂ cooling for the optical bench and detectors. In order to keep the instrument background below the HxRG detector dark current (~ 0.1 electron/sec), LN₂ cooling of the cold structure is done. The radiation shield which surrounds the cold structure is cooled by using a closed-cycle cooler. A cooling temperature of ~ 150 K is sufficient for the radiation shield to reduce the radiation load on the cold structure which can be managed very easily by the LN₂ can. The surface areas of the cold structure, radiation shield and the vacuum jacket are 1.8 m², 2.6 m², and 4.3 m², respectively.

We have used a CTI model 9600 high voltage compressor[§] manufactured by Brooks, USA[¶] along with two long (40 meters each) pressurized Helium lines to cool the highly polished 5 mm thick 6061-aluminum radiation shield to less than 150 K. The estimated heat load on the cold structure consists of 2.1 W heat from the radiation shield having temperature of 150 K, 1.9 W from the holes in it (entrance window etc), 1.7 W from

[‡]<https://www.animatics.com/>

[§]https://www.idealvac.com/files/manuals/Brooks9600High_1.pdf

[¶]<http://www.brooks.com>

support V-trusses, 1 W from the wiring, and 0.25 W from the motor shafts. The expected variation in the performance of the closed-cycle cooler does not effect the temperature of the cold structure as its heat load is negligible. The temperature variation due to the boil-off of the LN_2 (~ 0.5 K) is also small to affect the instrument performance (e.g., instrument background or focus).

The instrument can cool-down in ~ 60 hours and the hold time for the 14.16 L capacity LN₂ can is ~ 100 hours within the ambient temperature range of 283 to 301 K. Optical bench and guide detector are maintained at 76 ± 2 K. Warm-up also takes 60 hours, but by bowing out the LN₂ by circulating dry air, the cryostat can be warmed up faster .

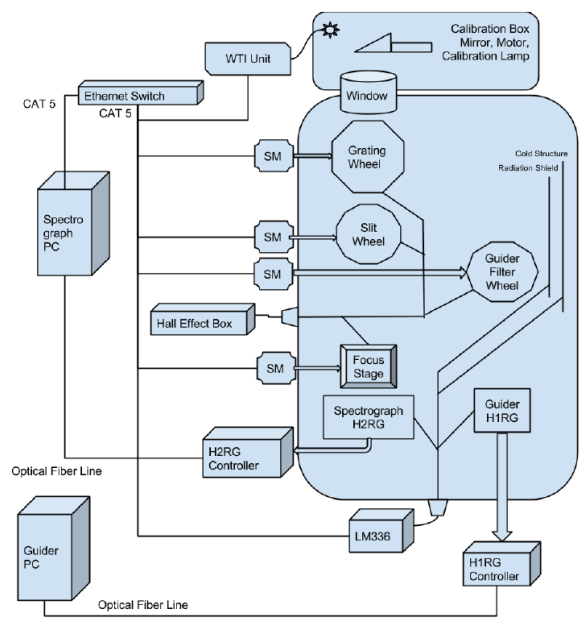


Figure 9. The representative scheme of the TANSPEC Hardware. Apart from a PC (for both guider and spectrograph), all other components are mounted on the telescope either on electronics rack or on the cryostat of the TANSPEC.

5. Electronics and Control System

Overall scheme of the TANSPEC hardware is shown in Fig 9. All instrument electronics along with the instrument are mounted at the telescope Cassegrain port. It consists of the array controllers for the two detectors, preamps, analog-to-digital (A/D) boards, DSP boards, remote Ethernet power control of all elements, mechanism drivers, temperature control monitoring of all parameters, Ethernet switch, power supplies, etc., which are controlled by the Unix Workstations placed in the control room and connected through optical fibers. The wheels, H2RG focus mechanics and calibration box mirror are moved using independent smart motors. The motors are controlled through a standard Ethernet interface. Electronics cabinet is insulated and designed

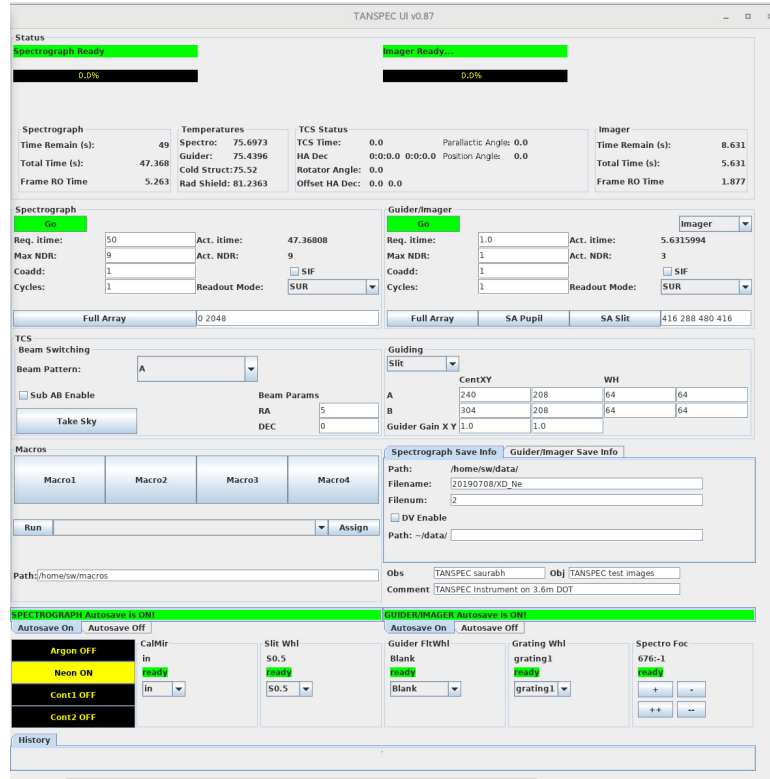


Figure 10. The TANSPEC graphical user interface (GUI). It provides control to the TANSPEC by using various buttons, icons, menus, and macro files.

for glycol cooling to ambient temperature using glycol chillers. The detector arrays are controlled by ARC Gen III controllers (H2RG: 4 channels and H1RG: 1 channel) from ARC, Inc., USA^{||}. It is also known as Leach Controller or San Diego State University (SDSU) Controller. The configuration of the arrays and its controllers are similar to our previous instrument ‘TIRSPEC’ (see for details, [5]). All the temperatures (arrays, radiation shield and cryostat) are monitored using a Lakeshore temperature controller (Model No: 336). The electrical connections and the chassis for the spectrograph controller have provisions to increase the channels to 32 in case 32 output mode of the H2RG is required at a later stage.

6. Software

The computer in the observing room hosts software to communicate and control individual components such as arrays, mechanism motors, lamps, etc. The software is also interfaced with the Telescope Control System (TCS) and has guiding capabilities. It also fetch header information from the TCS. It has Temperature Control Software for the spectrograph detector and Temperature Monitor Software for the optical bench and Guide Detector. All the mechanism can be controlled/powered ON through this

^{||}<http://www.astro-cam.com/Gen3Products.php>

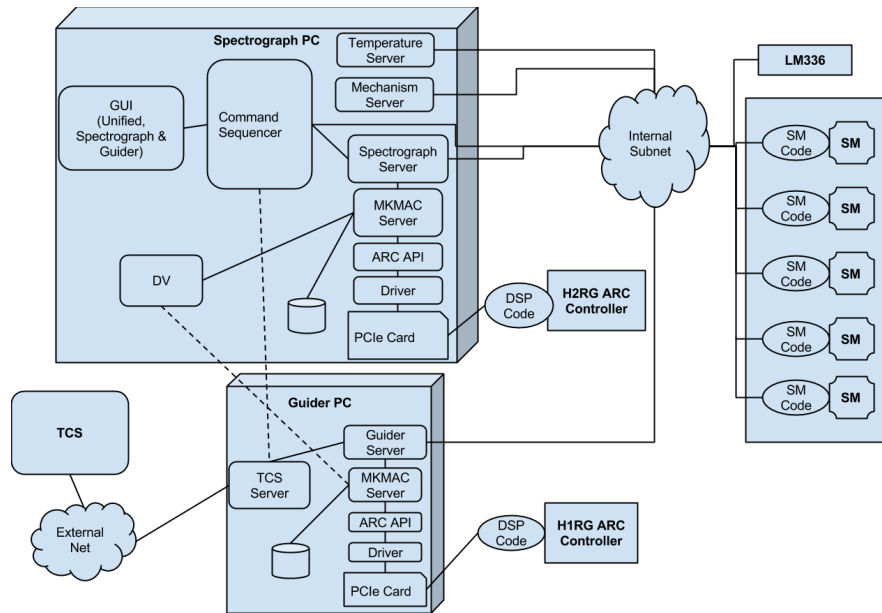


Figure 11. A representative scheme of the TANSPEC software. A PC (both for spectrograph and slit-viewer/guider) is placed in the observing room with different servers, PCI cards, and software. The PC is also connected with TCS (for its feedback/control), array controllers, different mechanisms, etc.

Software along with capabilities to do Scripting and Macros. In Fig 10, we show the screen-shot of the GUI of the TANSPEC which provides control to the TANSPEC by using various buttons, icons, menus, and macro files.

The overall structure of the TANSPEC software (see also, [5]) is shown in Fig 11. The central server is the command sequencer and it communicates and control other servers via UNIX style sockets. The command sequencer receives the command from the GUI and sends corresponding instructions to other servers (e.g., mechanism server, Array Controller Server (ACS), etc), and then, returns instrument status to the GUI. The mechanism server and ACS sends commands to the, Animatics Smart-Motor via the Ethernet link, and ARC controller via the ARC application programming interface (API), respectively. After the data is fully written to the system memory, PCI board sends interrupt command to the Central Processing Unit (CPU) and ACS generates Flexible Image Transport System (FITS) image from the raw data and saves it to the hard disk. It also sends the data via a socket to the quick look viewer software DV, data viewer by NASA Infrared Telescope Facility (IRTF), Hawaii, USA**. DV has a capabilities to do basic image arithmetic as well as quick measurements to check image quality.

**<http://irtfweb.ifa.hawaii.edu/Facility/DV/>

7. Detectors and its performances

Two science grade detectors, H2RG and H1RG, procured from Teledyne, USA^{††} are used in the spectrograph and slit-viewer, respectively. Their characterization results are provided below.

7.1. Readout mode and image generation

The array is continuously reset pixel by pixel when an exposure is not being taken. When an exposure is requested the present background reset is completed and then the requested exposure is done. This reduces the after image and avoids hard saturating array and also it sets up a consistent thermal cadence and reduces the thermal anomaly effect. The detector can be read out in various modes, i.e. Single Read, Double Correlated Sampling and the Sample-Up-The-Ramp (SUTR). The SUTR is the recommended mode of readout as there will be reduction in the readout noise due to the multiple sampling of the ramp values which reduces the readout noise to about 5 electrons. The SUTR readout technique is also useful when the pixels saturated or are hit by cosmic rays (see for details, [5]). The flux rate in each pixel is calculated by fitting a line to the counts along the time axis on the SUTR readout data cube. The H2RG array has sub-array capabilities in Y-axis, whereas, the H1RG has this capability in both the X and Y axes of the array. There is also in-built software to guide on slit image and send corrections to TCS Software to guide on-field objects. In H2RG array, four vertical-strips are read out simultaneously at a rate of $\sim 5 \mu\text{s}$ per pixel and in total, 5.263 seconds are required to complete one full frame read out. Therefore, the exposure time is adjusted automatically to the nearest multiple of 5.263 second (non-destructive readouts of the cumulative counts) and is written to the header of the image file. For H1RG array, it take 1.877 seconds to readout the frame and therefore, the actual exposure time is adjusted to the multiple of 1.877 second. In the top panel of Fig 12, we show the image and distribution of the counts for the first readout of the H2RG array. As the H2RG is readout via 4 channels, we can see four strips for that in the image. A broad intensity distribution with high values as expected in the bias level of NIR detectors is seen. In the lower panel of Fig 12, the same has been shown for the second readout by subtracting the first readout. The sampling clearly shows a Gaussian distribution with mean around zero and sigma of ~ 25 Analog to Digital Unit (ADU) which is equivalent to the readout noise of the H2RG array in low-gain setting.

7.2. Gain

We have taken many frames of different exposures with the array exposed to the continuum lamp (for H2RG) and to the telescope enclosure with $Br\gamma$ filter (for H1RG). Then, for each pixel, we have plotted the counts and its variance (also know as photon transfer curve) and calculated the slop. The inverse of this slope will be the gain value

^{††}<https://www.teledyne.com/en-us>

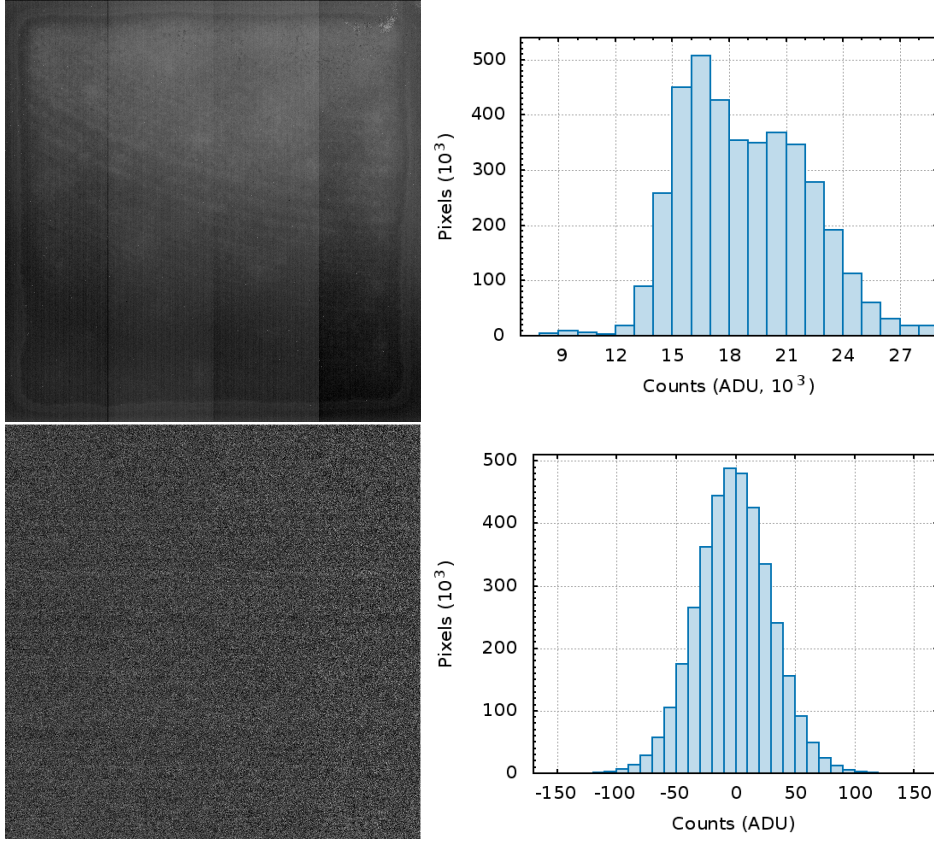


Figure 12. Upper panels: Image and histogram of the first readout (bias level) of the dark image for the H2RG array in high gain setting. Lower panels: Similar as above but for the second readout after subtracting the first readout.

(see for details, [5]). We have selected different regions of box size 5×5 pixels of the exposed area, totaling to ~ 500 pixels, of both H1RG and H2RG arrays for the gain calculation. Fig 13 shows the histograms of the gains obtained for both H2RG and H1RG arrays. We have fitted a Gaussian function on these distributions and found the peak gain values as $4.5 \pm 0.2 e^-/\text{ADU}$ and $4.3 \pm 0.2 e^-/\text{ADU}$ for the H2RG and H1RG arrays, respectively. In high-gain setting of the H2RG array, we have found peak gain value of $\sim 1.12 \pm 0.03 e^-/\text{ADU}$.

7.3. Dark Current

Dark current is estimated by putting cold block filter in the filter wheel (for H1RG) or the mirror in the slit wheel (for H2RG) and reading out the array. In the left panel of Fig 14, we show the variation of the counts in the dark frame as a function of time for the H2RG (for both high-gain and low-gain settings) and the H1RG arrays. A straight line fit to this distribution gave a dark current value of $\sim 0.016 \text{ ADU/sec}$ and $\sim 0.013 \text{ ADU/sec}$ for H2RG (low-gain) and H1RG arrays, respectively. This multiplied by gain-values gives us an estimate of the dark current as $\sim 0.07 e^-/\text{sec}$ and $\sim 0.06 e^-/\text{sec}$. Similarly, in the high-gain setting of the H2RG array, the dark current is $\sim 0.07 e^-/\text{sec}$.

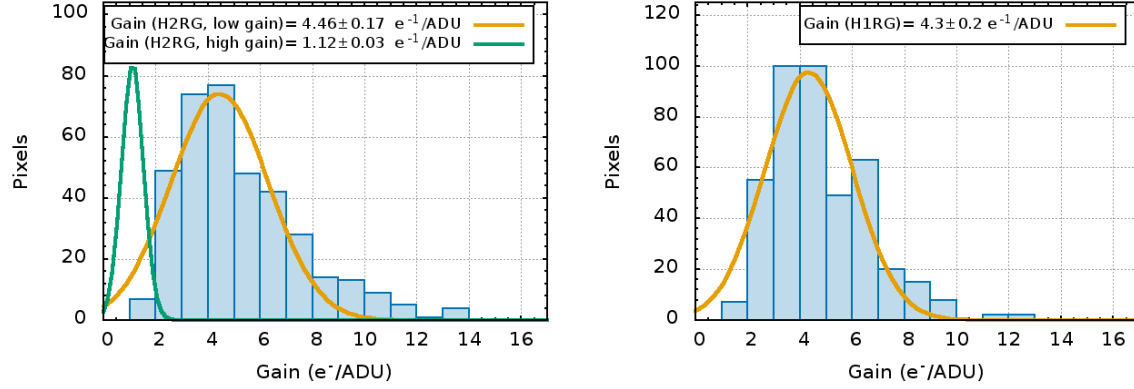


Figure 13. Distribution of Gain values for the H2RG array in low/high-gain settings (left panel) and for the H1RG array (right panel). The thick line is a Gaussian fitted curve on the distribution.

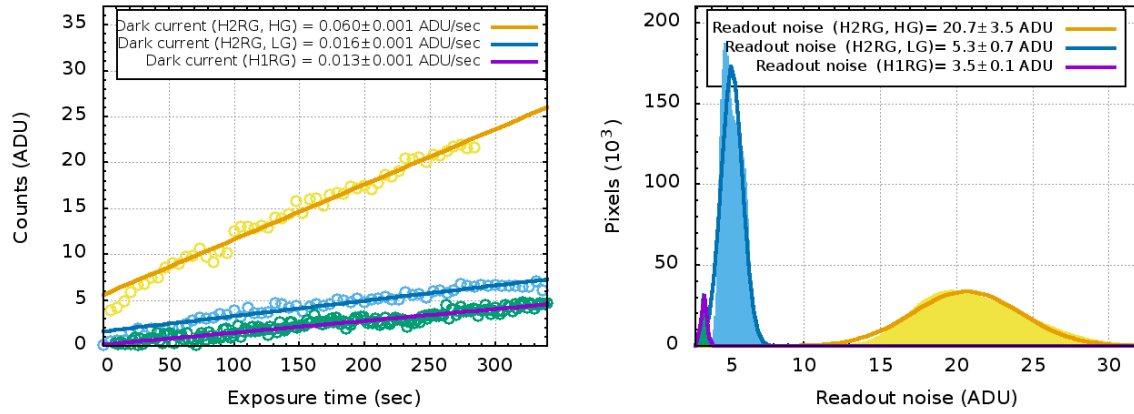


Figure 14. Dark current (left panel) and readout noise (right panel) for the H2RG array in both high-gain (HG) and low-gain (LG) settings and for the H1RG array.

Few sets of dark frame readouts at the beginning and end of each night would be enough for its correction.

7.4. Readout Noise

Since dark current is very small, for the readout noise calculation, we have used set of frames generated from the difference of consecutive frames of a dark exposure. We have calculated the standard deviation in the count values for each pixel in the above set of frames. This standard deviation is actually $\sqrt{2}$ times readout noise value of each pixel (see for details, [5]). The distribution of the readout noise for all pixels in the arrays are shown in the right panel of Fig 14. The readout noise for the H2RG (low-gain) and H1RG arrays is found be 5.3 ± 0.7 and 3.5 ± 0.1 ADUs, respectively. In the high-gain setting of the H2RG, the readout noise is estimated as 20.7 ± 3.5 ADUs. Here, it is worthwhile to mention that the above readout noise values are for a single readout. The

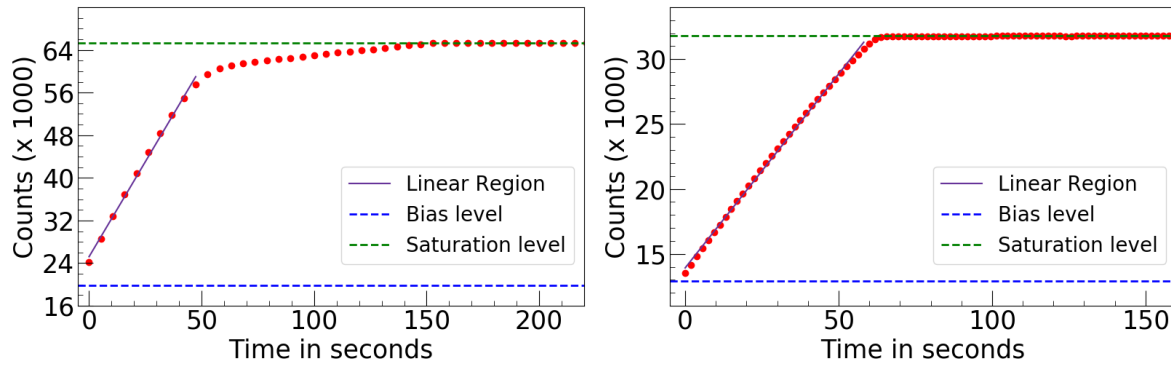


Figure 15. Linear range and the saturation values for the H2RG (left panel) and H1RG (right panel) arrays.

readout noise is a function of the number of readouts and will decrease with increase in the number of readouts, e.g., in case of H2RG, the readout noise will be 1.2 ADUs for 284 readouts (or 5.3 e^- , low gain setting). For more details please see [6].

7.5. Linear range and Saturation levels

Using the SUTR readout data of continuum lamps (for H2RG array) and Argon lamp with $\text{Br}\gamma$ filter (for H1RG), we have estimated the median saturation level of these arrays as ~ 28000 ADU (~ 65000 ADU for high gain) and ~ 32000 ADU, respectively, for low gain setting. In Fig 15, we show the variation of the median intensity value as a function of exposure time for these arrays for low gain setting. We can clearly see the saturation levels along with the non-linearity in the curves near these limits. We have estimated the median value of the upper limit for the linear regime of H2RG and H1RG arrays as 26000 ADU (57000 ADU for high gain) and 30000 ADU, respectively. As the median bias level for the H2RG and H1RG arrays are at ~ 20000 ADU (20000 ADU for high gain) and ~ 13000 ADU, the effective (useful) well depths for these arrays are found to be at the level of ~ 6000 ADU (~ 37000 ADU for high gain) and ~ 17000 ADU, respectively, in low gain setting. Here, it is worthwhile to mention that very bright spectral lines or stars can result in residual images that can contaminate the darks.

7.6. Bad, Hot and Cold pixels

The pixels which deviate more than 8σ from the median value in the image which is generated by dividing two flats (taken in low and high incident flux), are defined as bad pixels. The percentage of the bad pixels in the H1RG array is 0.03%, most of which are along the edges. For the H2RG array, which is used for spectroscopy, the different orders observed in continuum lamps were used to detect bad pixels which are negligible in numbers.

The pixels having counts more than 8σ above the median value in a dark readout of 100 sec are defined as hot pixels. The fraction of hot pixels for the H1RG and H2RG

Table 4. Main parameters of the detectors used in the TANSPEC instrument.

Parameter	H2RG (high-gain)	H2RG (low-gain)	H1RG
Number of pixels	2048 \times 2048	2048 \times 2048	1024 \times 1024
Pixel size (μm)	18	18	18
Gain (e^-/ADU)	1.1	4.5	4.3
Readout noise (ADU)	20.7 ± 3.5	5.3 ± 0.7	3.5 ± 0.1
Dark Current (ADU/sec)	0.060 ± 0.001	0.016 ± 0.001	0.013 ± 0.001
Saturation (ADU)	65000	28000	32000
Use full well-depth (ADU)	37000	6000	17000
Readout time (sec)	5.263	5.263	1.877
Readout channels	4	4	1
Sampling	Single read, Up the Ramp, Double Correlated Sampling, Non Destructive Reads (NDRs)		same
Sub-array capability	In Y -axis	In Y-axis	In both X and Y axes

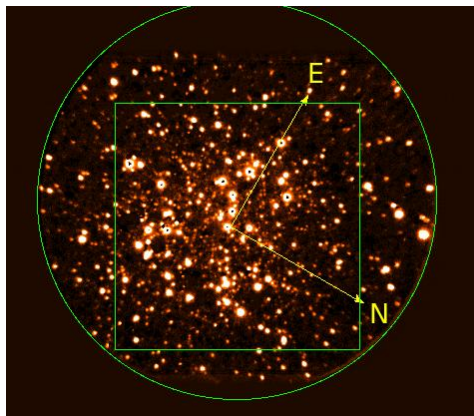


Figure 16. Image of a Globular cluster M53 taken in the K_s band using the slit-viewer of the TANSPEC on 3.6-m DOT on 20 April 2019. The sub-array of the H1RG array is used to image a circular FOV of sky having radius of 49 arcsec (shown as a green circle) through a mirror in the slit wheel and a filter in the filter wheel. The image quality of the FOV is optimized for the $60'' \times 60''$ FOV (shown as a green box). The FOV of the slit viewer is rotated by 120 degrees in clockwise direction which can be aligned by off-setting rotator of the telescope by 120 degrees.

arrays was found to be 0.05% and 0.03%, respectively. They are distributed randomly over the arrays. Similarly, cold pixels (pixels which have counts less than 8σ below median value in a dark readout of 100 seconds) fraction was found to be negligible for both the arrays.

The main parameters of the H2RG and H1RG arrays used in the TANSPEC instrument are listed in Table 4.

8. Performance on the 3.6-m DOT

Ground testing of the TANSPEC was carried out during the first week of April 2019 and subsequently it was mounted on the 3.6-m DOT. The TANSPEC was then used for on-sky commissioning tests during April - May, 2019. We present initial results in the following sub-sections.

8.1. Observing procedure

The detailed procedure for observing through the TANSPEC is provided in the TANSPEC observation manual.^{‡‡} Briefly, the observer selects the required slit and spectroscopy mode (XD mode or prism mode) through slit wheel and grating wheel, respectively. A desired filter can be selected through the filter wheel and the target source is then imaged in the slit viewer/guider. Afterwards, the target source is placed in the center of the slit by giving off-sets to the telescope. Guiding can also be done with the slit viewer through any filter (optical to NIR) on an object in its FOV. The magnitude limit for auto-guiding is roughly about $J \sim 10$ mag in an exposure of 10 s. Telescope's visible guider can also be used to guide stars. Once guiding is started, long integration of several hundred seconds can be done on the faint sources. In order to correct the spectra for the sky lines, telluric standards should be observed near to the target source at about similar airmass. Calibration frames such as arc-lamps, dark, flats are usually taken at standard star position by executing a calibration macro. All updates and information about the TANSPEC instrument are provided at ARIES 3.6-m DOT instrument page.^{§§} The initial version of the data reduction pipeline, pyTANSPEC^{¶¶}, which supports the XD mode data reduction for slits of width 0.5 and 1.0 arcsec is also released.

8.2. Imaging: Slit-viewer

By using the slit-viewer in the TANSPEC mounted on the 3.6-m DOT, we can image celestial objects on the H1RG array.

8.2.1. Field-of-view, Plate Scale and Image Quality Image of a Globular cluster M53 taken in the K_s band using the slit-viewer of the TANSPEC on 3.6-m DOT is shown in Fig 16. The sub-array of the H1RG array is used to image a circular FOV of sky having radius of 49 arcsec (shown as a green circle in the Fig 16) through a mirror in the slit wheel and a filter in the filter wheel. The image quality is optimized for the $60'' \times 60''$ FOV (please refer Fig 16). Astrometry of the image of the astronomical objects obtained by using the slit-viewer was done by using the Graphical Astronomy and Image Analysis Tool^{***} with a rms noise of the order of ~ 0.25 arcsec. The plate scale was estimated as $0.245''/\text{pixel}$. The FOV the slit-viewer is rotated by 120 degrees in clockwise direction which can be aligned in the celestial north-south direction by off-setting rotator of the telescope by 120 degrees.

An example of typical stellar profiles in K_s and r' bands using the slit-viewer on the TANSPEC are shown in Fig 17. We have observed several regions in photometric

^{‡‡}<https://aries.res.in/sites/default/files/files/3.6-DOT/Tanspec-Observation-Manual.pdf>

^{§§}<https://aries.res.in/facilities/astronomical-telescopes/360cm-telescope/Instruments>

^{¶¶}<https://github.com/astrosupriyo/pyTANSPEC>

^{***}<http://star-www.dur.ac.uk/~pdraper/gaia/gaia.html>

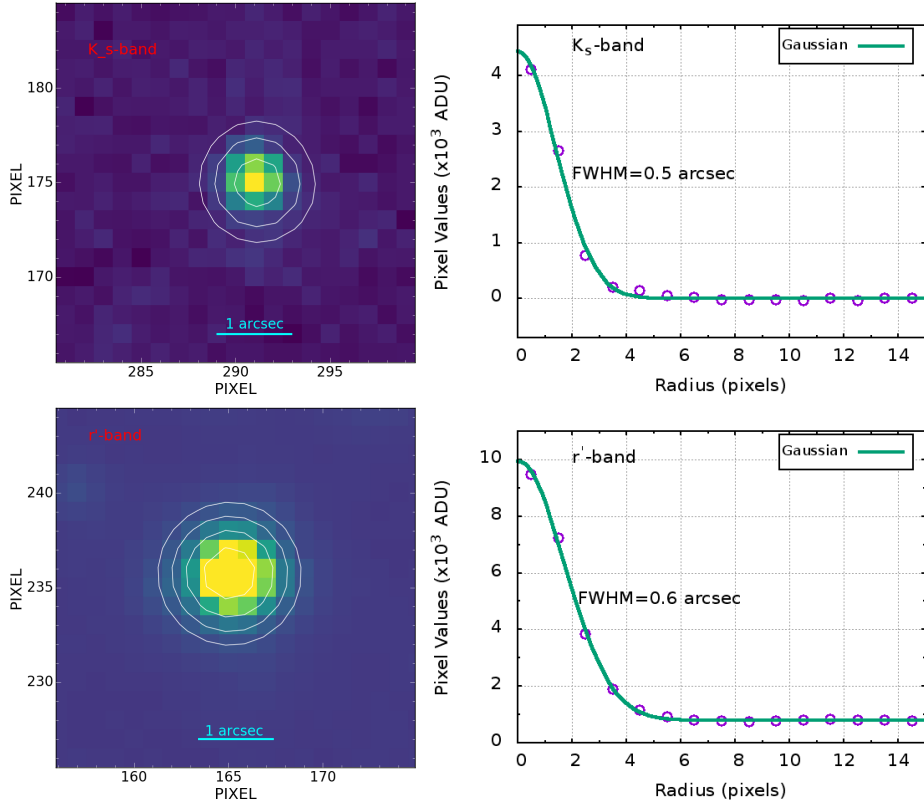


Figure 17. Shape and radial profile of stars in K_s (upper panels) and r' (lower panels) bands using the slit-viewer on the TANSPEC. The full width at half maximum (FWHM) of the stellar profile is 0.5 arcsec and 0.6 arcsec in K_s and r' bands, respectively.

nights to check for the variation of the full width at half maximum (FWHM) in different directions. The size (FWHM) of the point spread function (PSF) of the stellar images is found out to be around ~ 0.45 - 0.60 arcsec in the K_s -band ($2.2 \mu\text{m}$) and ~ 0.6 - 0.7 arcsec in the r' -band ($0.61 \mu\text{m}$). This is in accordance to the wavelength dependence of the atmospheric seeing.^{† † †} The images are also found to be circular in shape (ellipticity = $0.02 - 0.2$). There is no direction dependent variation in the PSF of the stellar images.

8.2.2. Color equations We took NIR observations of a field near W51 star-forming complex ($\alpha_{2000} = 19^{\text{h}}25^{\text{m}}40^{\text{s}}$, $\delta_{2000} = +15^{\circ}07'46''$) with four frames of 10 sec exposure in each of the 5-point dither pattern in J , H , and K_s filters. We also did observation of an open cluster Be 20 ($\alpha_{2000} = 05^{\text{h}}32^{\text{m}}36^{\text{s}}$, $\delta_{2000} = +00^{\circ}11'19''$) in optical r' and i' bands with 12 frames of 5 minutes exposures, i.e., a total of one hour exposure in r' and i' filters. Dark frames and sky flats were also taken during the observations. The sky frames in NIR filters (JHK_s) were generated by median combining the dithered frames. The basic image processing such as dark/sky subtraction and flat fielding was

^{† † †}https://www.astro.auth.gr/~seeing-gr/seeing_gr_files/theory/node17.html

done using tasks available within Image Reduction and Analysis Facility (IRAF)^{‡‡‡}. Instrumental magnitudes were obtained using the DAOPHOT package. As the target region was crowded, we have carried out the PSF photometry to get the magnitudes of the stars. The obtained color correction equations for NIR filters (JHK_s) of the TANSPEC on the 3.6-m DOT for calibrating to Two Micron All Sky Survey (2MASS) magnitudes are as follows (see also, [7]).

$$(J - H) = (0.91 \pm 0.07) \times (j - h) + 0.05 \pm 0.08 \quad (1)$$

$$(H - K) = (1.01 \pm 0.07) \times (h - k) + 0.51 \pm 0.05 \quad (2)$$

$$(J - K) = (1.17 \pm 0.05) \times (j - k) - 0.70 \pm 0.12 \quad (3)$$

$$(J - j) = (0.004 \pm 0.04) \times (J - H) - 1.21 \pm 0.04 \quad (4)$$

where, JHK are the standard magnitudes of the stars taken from the 2MASS catalog [8] and jhk are the present instrumental magnitudes of the same stars normalized per sec exposure time.

The color correction equations obtained for optical filters (r' and i') of the TANSPEC on the 3.6-m DOT for calibrating to the Panoramic Survey Telescope and Rapid Response System (Pan-STARRS1 or PS1 [9]) are obtained as follows.

$$(r_{P1} - i_{P1}) = (0.99 \pm 0.03) \times (r - i) - 0.06 \pm 0.01 \quad (5)$$

$$(r_{P1} - r) = (0.08 \pm 0.06) \times (r_{P1} - i_{P1}) - 6.14 \pm 0.02 \quad (6)$$

$$(i_{P1} - i) = (-0.01 \pm 0.01) \times (r_{P1} - i_{P1}) - 6.05 \pm 0.02 \quad (7)$$

where, r_{P1} and i_{P1} denote the standard magnitudes of the stars taken from the PS1 data release 1 catalog^{§§§}, and r and i are the present instrumental magnitudes of the similar stars normalized per sec exposure time.

8.2.3. Sensitivity To estimate the photometric sensitivity, we took deep NIR observations of an open cluster Teutsch 76 ($\alpha_{2000} = 22^h 28^m 47^s$, $\delta_{2000} = +61^\circ 37' 55''$) with five frames of 20 sec exposure in each of a 7-point dither pattern in J , H , and K_s filters. We took 5 sets of these observations which gives a total exposure time of ~ 1 hour in J , H , and K_s filters. For optical bands, we have used the deep data of an open cluster Be 20 with an hour exposure each in r' and i' filters, as discussed in the previous section. Individual cleaned images were average combined to give the final image on which we have done photometry as per the procedure mentioned in the previous section. The FWHMs of the stellar profile in these final images were around ~ 0.8 arcsec (NIR bands) and ~ 1 arcsec (optical bands), respectively. The observations were carried out

^{‡‡‡}IRAF is distributed by the National Optical Astronomy Observatory, which is operated by the Association of Universities for Research in Astronomy (AURA) under cooperative agreement with the National Science Foundation.

^{§§§}<http://catalogs.mast.stsci.edu/>

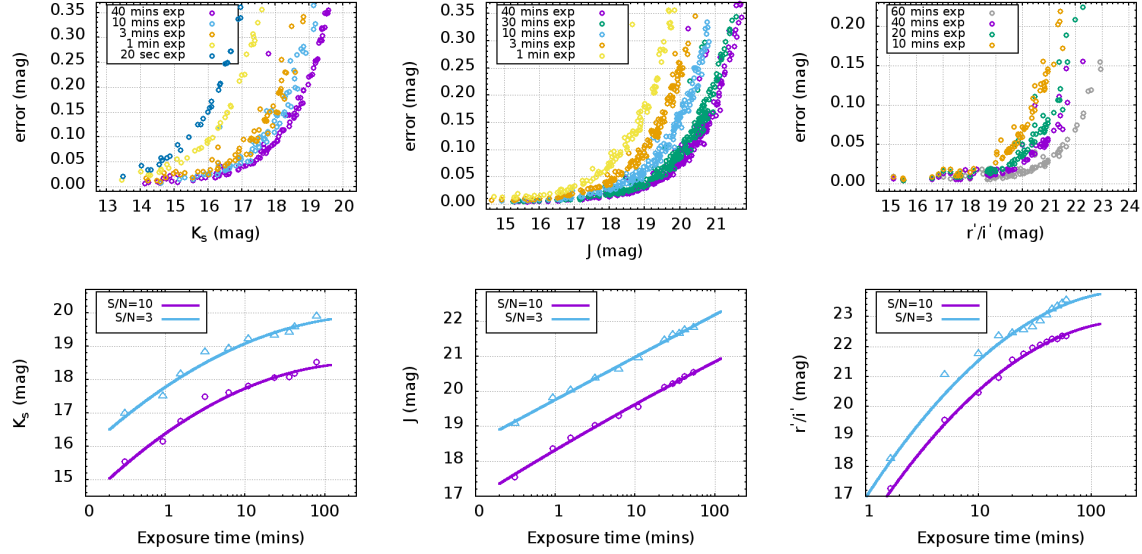


Figure 18. Sensitivity curves for the slit-viewer in the TANSPEC instrument. Top panels: Error as a function of magnitude in K_s , J , and r'/i' bands for different exposure times. Bottom panels: K_s , J , and r'/i' magnitudes as a function of exposure time for SNR = 10 and 3. The solid curves are the fitted function on the data points shown by open circles/triangles.

at an approximate elevation of 55-45 degrees. The humidity was around 40-60 %, and temperature ranges from 4 to 12 degrees Celsius.

The top panel of Fig 18 shows the magnitude versus error plot for different exposures for the stars in the cluster field in the IR and optical filters. Using these plots, we have generated the exposure time versus magnitude graphs in different filters for signal to noise ratio (SNR) = 10 and SNR = 3 (detection limit) and are shown in the bottom panels of the Fig 18. The curved lines are the polynomials fitted to the data points generated by the smoothed spline function on the observed data points. These curves are generated with an M1 reflectivity value of 90 %. Clearly, the TANSPEC has a sensitivity to detect faint source of $K_s \sim 19.7$ mag or $r' \sim 23.7$ (with an SNR of 3) in two hours of exposure. An exposure time calculator based on these curves is under development.

8.3. Spectroscopy: XD mode and prism mode

8.3.1. Wavelength range The calibration unit of the TANSPEC has Argon and Neon lamps for wavelength calibration and two continuum lamps for flat fielding the spectra taken in both XD and prism modes. The Argon lamp covers mostly the NIR part of the spectra whereas the Neon lamp covers mostly the optical part. Two continuum lamps, one at high voltage and another at low voltage, are used to cover all the orders of the spectra. The aperture on the integrating sphere is fine-tuned in such a way that the spectra do not get saturated in both modes of the TANSPEC.

In the top panels of Fig 19, we show the images of the Neon lamp (left panel) and the stellar spectra of an Wolf Rayet (WR) star ‘HD 16523’ (right panel) in the XD mode of the TANSPEC. These images were taken with 0.5 arcsec slit having 20 arcsec length. Exposure times for Argon/Neon lamps and an WR star ($K \sim 7.9$ mag) were 120/100 sec and 450 sec, respectively. All the orders starting from 3rd (1.86 - 2.54 μm) to 12th (0.55- 0.57 μm) are detected in both the lamps and stellar spectra. The spectra of an WR star clearly show the broad emission line features in almost all orders. The sky lines and thermal background at longer wavelengths ($\lambda \gtrsim 2.3 \mu\text{m}$) are also seen in the stellar spectra. The sky lines are mostly OH emission and can be subtracted by the spectra of a telluric standard. The thermal background can be due to several reasons, e.g., thermal emission from the telescope and dome structure, and can add noise in that part of the spectra. As can be seen from the images, all orders in the lamp spectra have sufficient lines that can be used to wavelength calibrate the stellar spectra. The lower panel of Fig 19 shows the extracted wavelength calibrated spectra for both lamp (left panel) and stellar (right panel) for all the orders. They also show the good coverage of lines required for wavelength calibration as well as various spectral features of an WR star. Wavelength calibration was done using the IDENTIFY task in IRAF with an accuracy of 0.1 μm and the reciprocal linear dispersion was $\sim 1\text{-}4 \text{ \AA/pixel}$.

Similarly, in the top panels of Fig 20, we show the images of the Neon lamp (left panel) and stellar spectra of a F-type star ‘HD 275142’ (right panel) in the prism mode of the TANSPEC. These images were also taken using the 0.5 arcsec slit having 20 arcsec length. Exposure times for Argon/Neon lamps and HD 275142 ($K \sim 9.7$ mag) were 3.5 sec and 150 sec, respectively. The lower panel of Fig 20 shows the extracted wavelength calibrated spectra for both lamp (left panel) and stellar (right panel) in the prism mode. From Figs 19 and 20, we can also see the full wavelength coverage of the instrument from 0.55 to 2.5 μm . Sky lines and thermal background are also evident in the spectra. No stellar features are seen at some wavelength regimes because of the atmospheric absorption due to H₂O and OH bands. Wavelength calibration was done with an accuracy of 0.4 μm and the reciprocal linear dispersion was $\sim 1\text{-}4 \text{ \AA/pixel}$.

8.3.2. Spectral Resolution The effective spectral resolving power of the spectra in each order was estimated by finding FWHMs of Argon/Neon lamp lines through the slits of 0.5 arcsec and 1.0 arcsec widths. Fig 21 shows the spectral resolving power ($\lambda/\Delta\lambda$) as a function of wavelength for 0.5 arcsec and 1.0 arcsec slits as obtained from the Argon/Neon lines in the XD mode (left panel) and the prism mode (right panel) of the TANSPEC. The median resolution in the XD mode is estimated as 2750 and 1600 for 0.5 arcsec and 1.0 arcsec slits, respectively. For the prism mode, the resolution varies from 100 (50) to 400 (250) for the 0.5 (1.0) arcsec slit across different regions of the spectra, respectively.

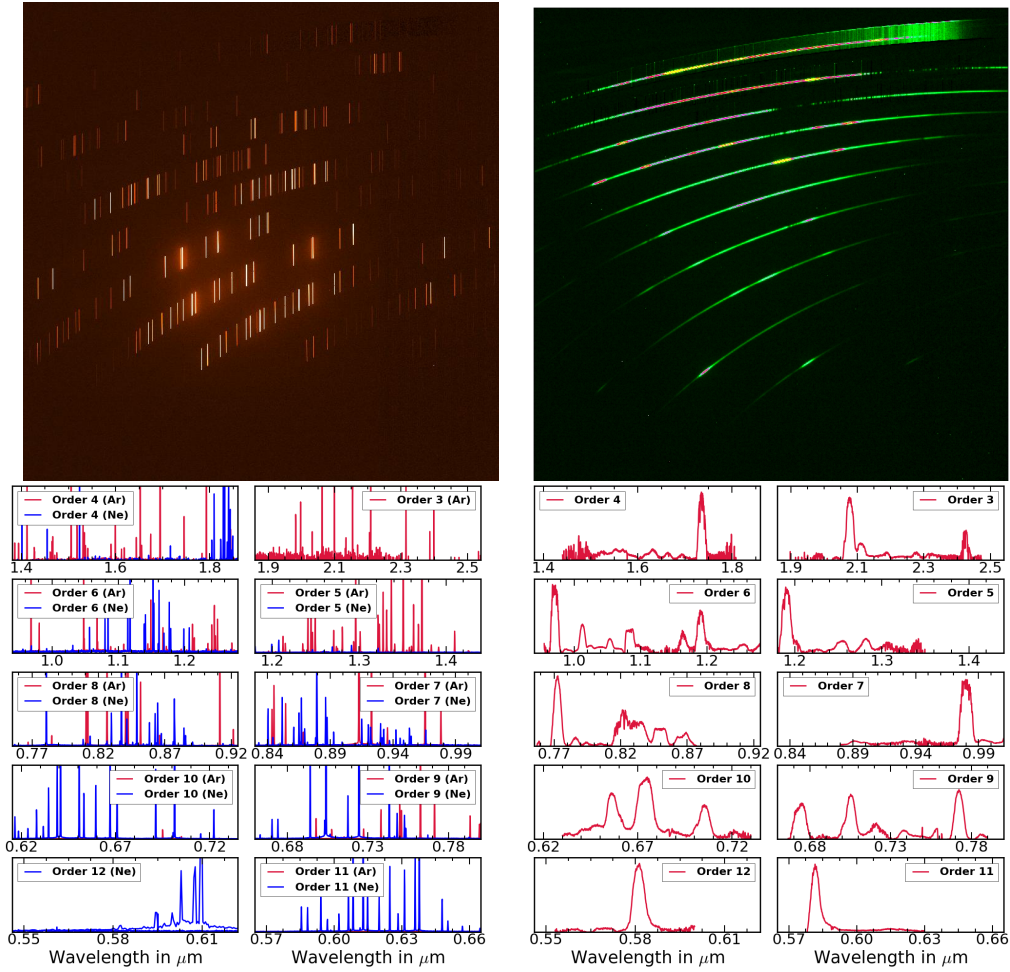


Figure 19. Images of the Neon lamp spectra (top left) and the spectra of an WR star, ‘HD 16523’ (top right) taken through TANSPEC in the XD mode. The wavelength calibrated spectra in different orders of the XD mode of the TANSPEC for Neon/Argon lamps (bottom left) and an WR star (bottom right).

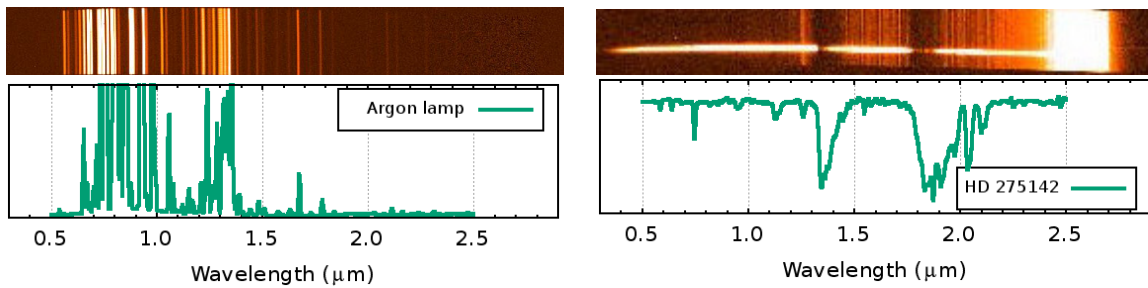


Figure 20. Images of the Argon Lamp spectra (top left) and F-type star ‘HD 275142’ spectra (top right) taken through the TANSPEC in the prism mode. The wavelength calibrated spectra in the prism mode of the TANSPEC for Argon lamp (bottom left) and ‘HD 275142’ star (bottom right).

Table 5. Estimate of the throughput (in %) of the TANSPEC Instrument for best optics performance including the telescope mirrors, instrument mirrors/lens/prism/grating/substrate and the quantum efficiencies of the detector arrays at different wavelengths.

Bands (μm)	$r'(0.66)$	$i'(0.81)$	$Z(0.9)$	$Y(1.02)$	$J(1.22)$	$H(1.63)$	$K_s(2.19)$
Imaging mode	42	40	51	55	58	60	63
XD mode	22	20	26	28	29	31	33
Prism mode	37	33	42	45	48	52	36

8.4. Throughput

For the efficient throughput, the entire optics needed to work efficiently across the entire 0.55-2.5 μm range of the instrument. The theoretical estimates of the throughput of the TANSPEC instrument in different modes at different wavelengths are given in Table 5. These numbers are estimated for the best optics performance of the system including the telescope mirrors, instrument mirrors/lens/prism/grating/substrate and quantum efficiencies of the arrays at different wavelengths. However, these estimates can be treated as upper limits as they do not include the atmospheric transmission and the slit losses. As expected, there is a decrease in throughput at shorter wavelengths (r' and i' bands) due to the combination of decreasing quantum efficiency (QE) of the array (including its own single-layer anti-reflection coating) and decreasing efficiency of the Broadband Anti-Reflection (BBAR) coatings on the transmissive optics. The peak throughput of the XD mode is about $\sim 30\%$. On the other hand, the peak throughput of the prism mode ($\sim 50\%$) is far more than that of the XD mode. The imaging mode peak throughput is estimated as $\sim 60\%$.

The throughput of the entire system in the imaging mode was also measured from the total flux of standard stars in an area of 4 times of the FWHM of their profile. The imaging mode throughput percentage is $30 \pm 5\%$, $45 \pm 5\%$, $44 \pm 5\%$ and $35 \pm 5\%$ for the r' , J , H and K_s bands, respectively. The lower K_s band throughput is may be due to the higher background at these wavelengths, i.e. thermal background and atmospheric lines. These numbers also includes other parameters such as QE of the detector, instrument/telescope optics and the atmospheric turbulences. The throughput in spectroscopy mode is very difficult to measure as it involves placing the star at the exact center of the slit every time. However, the throughput in the prism and XD modes was measured on an A0V star through 1 arcsec wide slit. We used the J band region of the spectrum to calculate the throughput. The theoretical J band flux for the star was calculated using Pogson's relation* where the zero point of the magnitude is taken from literature [10]. This value was converted to photon counts by dividing it with the energy corresponding to the J band wavelength. The observed photon counts were converted to units of counts/ m^2/s by dividing it with the effective collecting area and the total integration time. The ratio of the observed values to the theoretical values are

$$*M=2.512*\log(F) + C$$

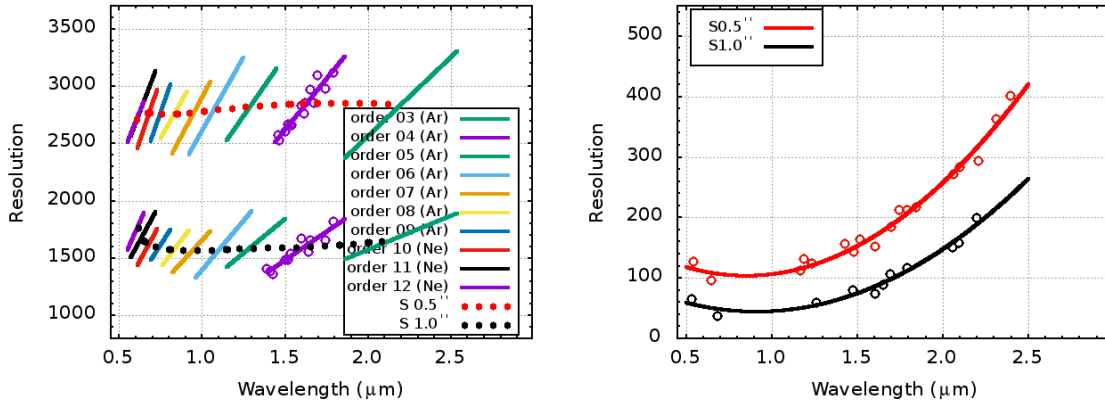


Figure 21. Spectral resolution as a function of wavelength in the XD mode (for different orders, left panel) and the prism mode (right panel) of the TANSPEC for 0.5 arcsec and 1 arcsec wide slits. The solid curves are fitted functions on the data points shown as open circles (for clarity, we have shown data points only for the 4th order in the XD mode).

obtained as 21% and 37%, which are the throughput values of the spectrograph in the XD and prism modes, respectively. As expected, the measured throughput values are lower than the theoretical estimates due to the atmospheric transmission and the current reflectivity of the primary mirror of the 3.6-m DOT, i.e., 45-60% in optical bands. Slit losses can also contribute to the low throughput values and a wider slit, e.g., 4'', can help to minimize those losses.

8.4.1. Sensitivity Sensitivity in spectroscopic mode is estimated by taking the spectra of A0V stars having a range of magnitudes. During observations, the stellar FWHM, relative humidity, temperature and the reflectivity of the M1 mirror of the 3.6-m DOT were 0.6-1.0 arcsec, < 60%, 5-15 degree Celsius and $\sim 50\%$, respectively. Fig 22 shows various estimates of exposure time required for a continuum SNR of 10 in different bands/orders of the XD mode as well as for the prism mode of the TANSPEC for the 0.5 arcsec and 1.0 arcsec wide slits. The SNR is quite sensitive to the FWHM of the star profile as well as the accuracy in centering of the star inside the slit. Therefore, the 1.0 arcsec slit provides better sensitivity than the 0.5 arcsec slit. We have found that the spectra of stars up to 15 mag (K_s), 17.5 mag (J), and 15.5 mag (R) can be observed in 2 hours of exposure with a 1.0 arcsec slit (with an SNR of 10) under typical night conditions. The SNR is also calculated from the extracted spectra of a $J=10$ mag A0V star in 0.5 arcsec and 1.0 arcsec slits and its variation with exposure time is also plotted in Fig 22 for the XD and prism modes of the TANSPEC. Deviation of the SNR from the \sqrt{t} line is possible when there are other sources of noise contributing on top of the photon noise. This can happen when counts are less, and the read noise is comparable to photon noise. The SNR at NIR bands are also prone to high background noises (thermal, atmospheric lines etc.) and can contribute to this deviation.

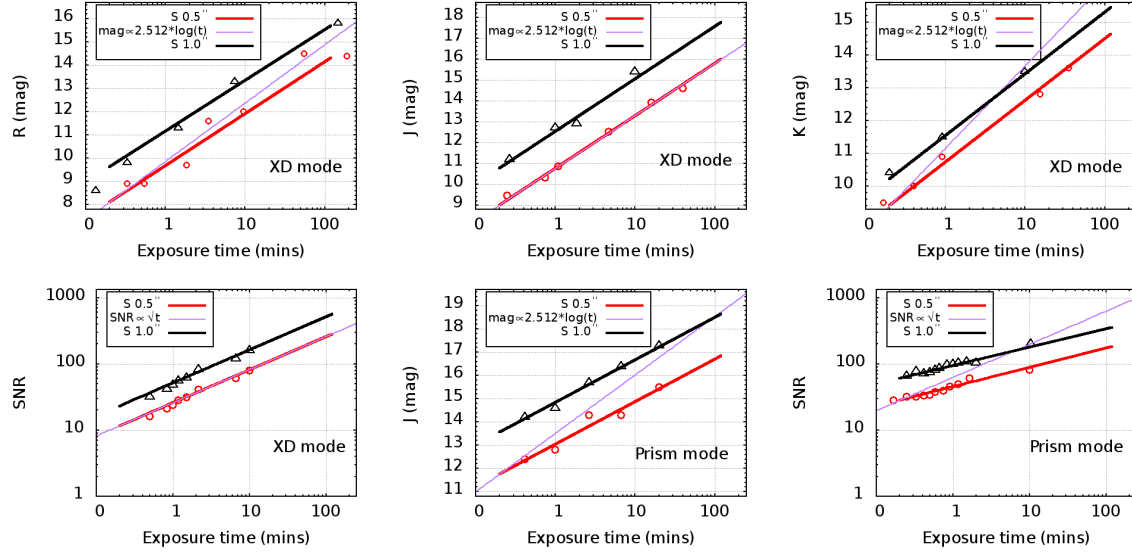


Figure 22. Sensitivity curves for the spectroscopic mode of the TANSPEC on the 3.6-m DOT. Thick lines are the magnitudes (for $\text{SNR} = 10$) and SNR versus exposure time curves for the XD mode and the prism mode of the TANSPEC for both 0.5 arcsec (red color) and 1.0 arcsec (black color) wide slits. Magenta lines are the scaling relationships ($\text{SNR} \propto \sqrt{t}$, $\text{mag} \propto 2.512 \cdot \log(t)$) normalized at short exposure time for the 0.5 arcsec slit. The thick curves are the fitted function on the data points shown by open circles/triangles.

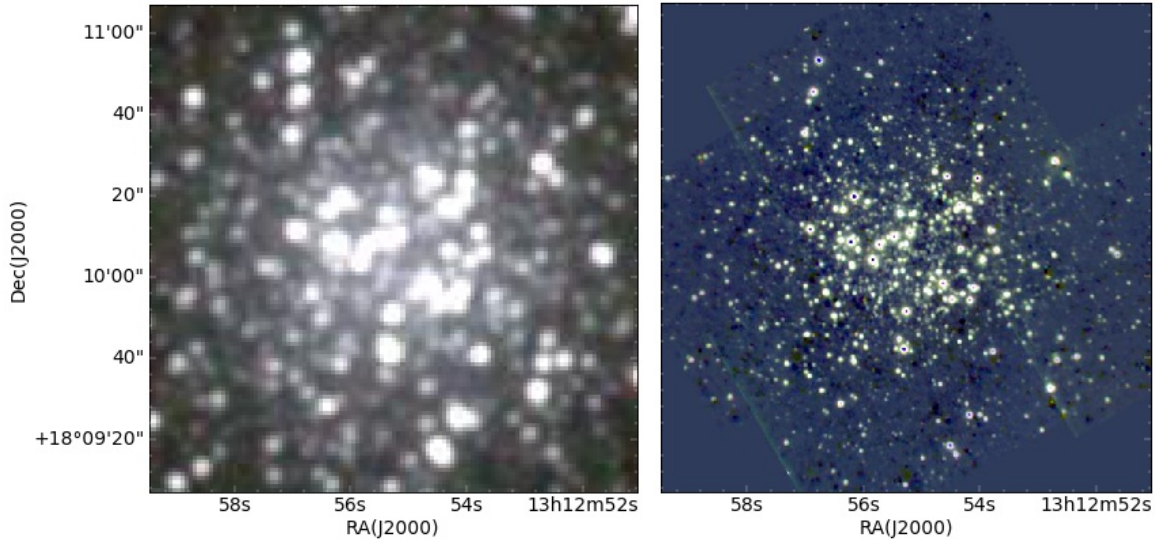


Figure 23. Comparison of the color-composite images of the $\sim 2' \times 2'$ FOV of the central region of M53 globular star cluster generated by using the K_s (red), H (green) and J (blue) bands images from 2MASS (left panel) and TANSPEC (right panel).

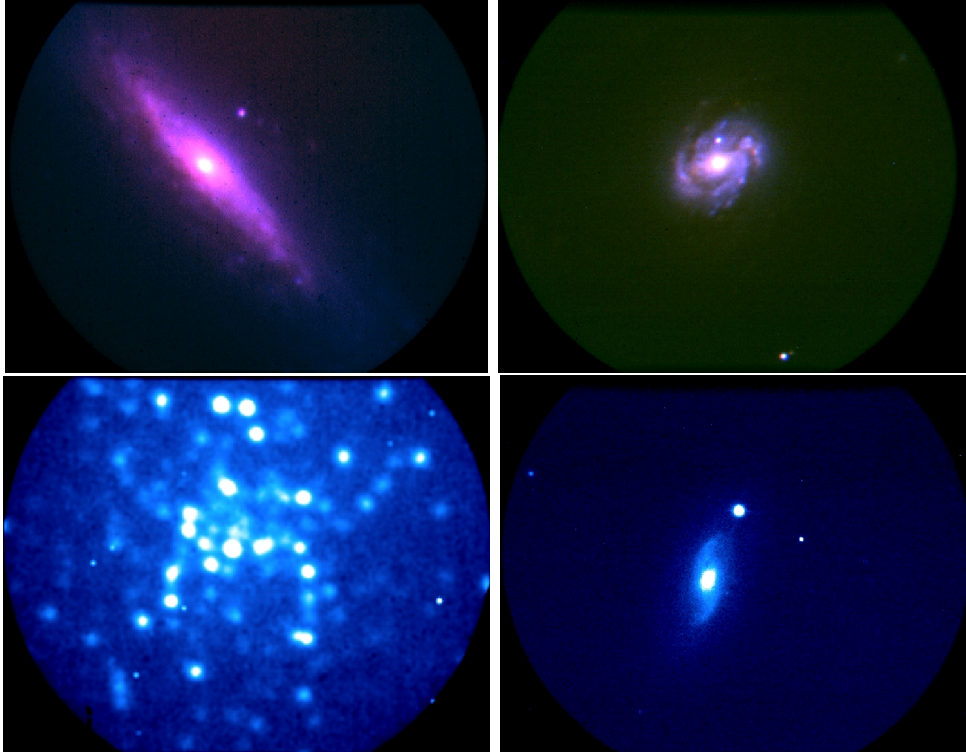


Figure 24. Color-composite images of galaxies NGC 4666 (top-left) and NGC 4328 (top-right) using J (blue), H (green) and K_s (red) images taken through the slit-viewer of the TANSPEC. J band images of a globular star cluster ‘Palomar 2’ (bottom-left) and a Seyfert galaxy ‘MCG+09-16-013’ (bottom-right) are also shown.

8.5. Example Images and Spectra

During the commissioning nights of the TANSPEC instrument, we have observed various astrophysical sources in the spectroscopy as well as imaging modes. We have done observations of M53 globular cluster using the slit-viewer in the TANSPEC on the 3.6-m DOT. As the FOV of the slit-viewer is small ($\sim 60'' \times 60''$), we have done observations of M53 in five pointings in J , H and K_s -band filters with 25 Non Destructive Reads (NDRs). The readout time of each NDR is 1.877 secs. In Fig 23, we show the comparison of the mosaiced image of the slit-viewer with that of 2MASS survey. We can easily see a better resolved and deeper image of the TANSPEC. Fig 24 shows color-composite images created from the J , H and K_s images and J band images of some of the sources observed with the TANSPEC. Fig 25 shows the optical-NIR spectra obtained from stars with different spectral types in both the XD and prism modes of the TANSPEC. The black curve is the atmospheric transmission at Mauna Kea.[†] The shaded regions are thus the regions where atmospheric features dominate the spectra and hence, we have not shown those wavelength ranges in our extracted spectra. We can easily identify various spectral features (marked as blue vertical lines) in both the spectra.

[†]<http://twiki.cis.rit.edu/twiki/bin/view/Main/MaunaKeaTo100kmAtmosphericTransmissions>

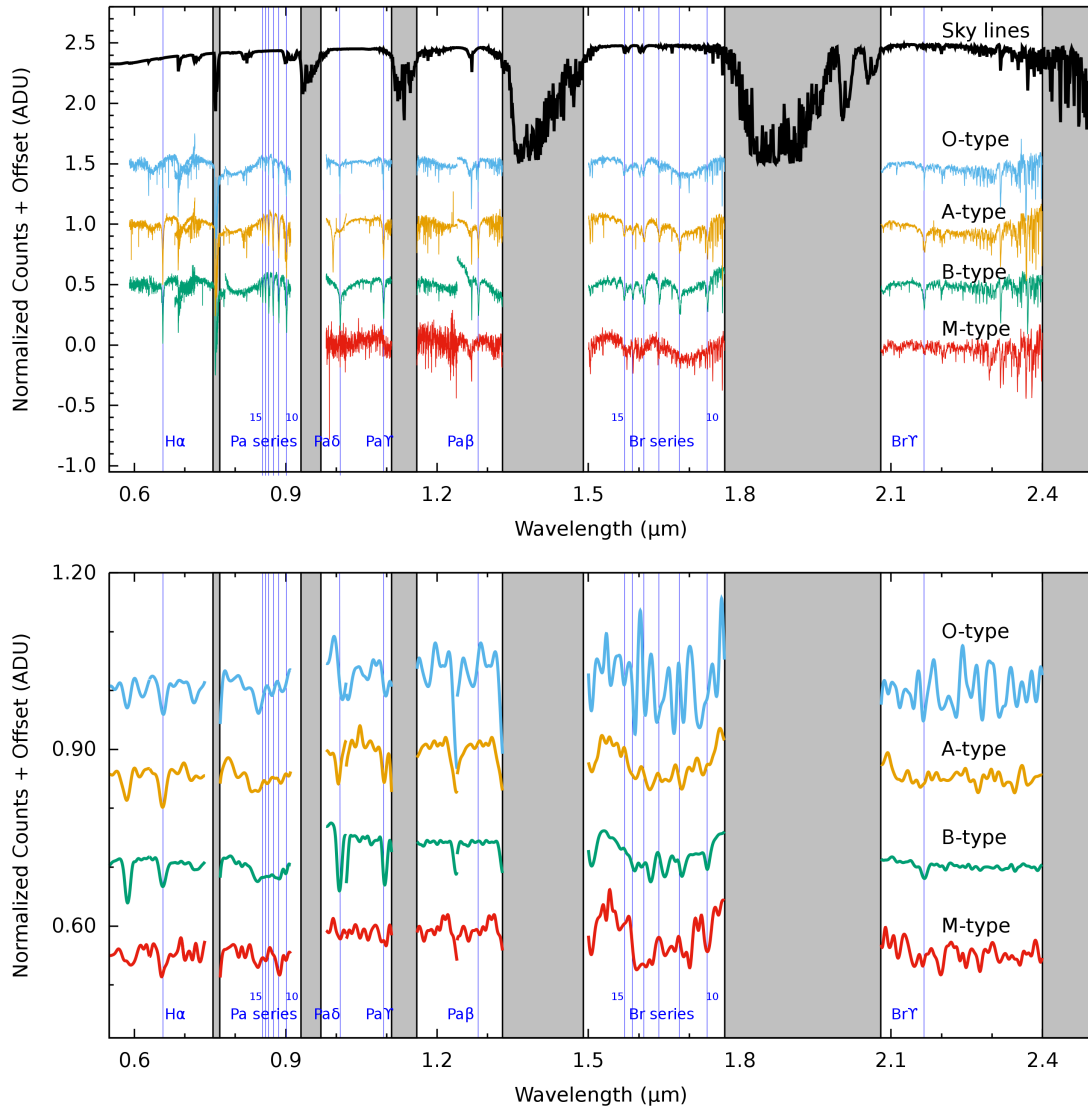


Figure 25. Sample spectra of stars of different spectral types in the XD mode (top panel) and the prism mode (bottom panel) of the TANSPEC taken with 0.5 arcsec slit. The shaded regions are the regions where atmospheric features dominate. Various detected spectral lines are also marked.

9. Conclusion

The TANSPEC is a unique instrument that has the ability to deliver simultaneous optical-NIR (0.55-2.5 μm) spectrum in a single exposure. The TANSPEC was delivered and commissioned on the 3.6-m DOT successfully. It has been used for both commissioning tests and science observations during 2019-2020. The two spectroscopic modes of the TANSPEC, XD mode and prism mode, provide spectra with resolutions $R \sim 2700$ and $R \sim 100\text{-}350$, respectively. The main parameters of the TANSPEC obtained during commissioning tests and science observations are tabulated in Table 6. It was officially released to the astronomy community in October 2020 and is currently being

Table 6. Main parameters of the TANSPEC Instrument.

Parameter	XD mode	Prism mode	Imaging
Wavelength coverage (μm)	0.55 - 2.5	0.55 - 2.5	0.55 - 2.5
Resolution ^a ($\frac{\lambda}{\Delta\lambda}$)	2750	~ 100 -400	~ 10
Plate scale (arcsec/pixel)	0.25	0.25	0.25
Throughput (% at J band)	30	48	58
Sensitivity ^b (mag)			
r'	15.7	17.0	22.5/20.5/16.0 ^c
i'	15.7	17.0	22.5/20.5/16.0
J	17.7	19.0	20.5/19.7/18.4
H	16.0	17.3	19.5/18.7/17.4
K_s	15.7	17.0	18.3/17.7/16.4

^a: for 0.5 arcsec slit. ^b: for 90% telescope reflectivity, 1 hr exposure, 1.0 arcsec slit, 1 arcsec seeing and SNR=10.

^c: 1hr/10min/1 min exposure.

used heavily for science observations by many astronomers worldwide.

Acknowledgments

We thank the staff of the 3.6-m DOT and 1.3-m DFOT, Devasthal (ARIES), for their co-operation during the observations. It is a pleasure to thank the members of the IR astronomy group (Department of Astronomy and Astrophysics) at TIFR for their support during observations. We acknowledge the Spex instrument[‡] which we relied heavily on for the initial concept and the many practical lessons learned from that instrument. The Project In charge (PI) and Co-PI of TANSPEC project are thankful to the funding agencies (Department of Science and Technology (DST) and Department of Atomic Energy (DAE), Government of India, India) for approving the project and Directors of TIFR and ARIES for their support and encouragement. Thanks to the ARIES Governing council and Project Management Board (PMB) (3.6-m DOT) for reviewing time-to-time the progress of the project, and finally, the DOT and TIFR teams for their support during installation and commissioning of the TANSPEC on 3.6-m DOT. Finally, TIFR team acknowledges the support of the DAE, Government of India, under project Identification No. RTI 4002.

References

- [1] Rayner J T, Toomey D W, Onaka P M, Denault A J, Stahlberger W E, Vacca W D, Cushing M C and Wang S 2003 *Publications of the Astronomical Society of the Pacific* **115** 362–382
- [2] Tokunaga A T, Simons D A and Vacca W D 2002 *Publications of the Astronomical Society of the Pacific* **114** 180–186

[‡]<http://irtfweb.ifa.hawaii.edu/~spex/overview/overview.html>

- [3] Bessell M S 1979 *Publications of the Astronomical Society of the Pacific* **91** 589–607
- [4] Rayner J T, Toomey D W, Onaka P M, Denault A J, Stahlberger W E, Watanabe D Y and Wang S I 1998 SpeX: a medium-resolution IR spectrograph for IRTF *Infrared Astronomical Instrumentation (Society of Photo-Optical Instrumentation Engineers (SPIE) Conference Series* vol 3354) ed Fowler A M pp 468–479
- [5] Ninan J P, Ojha D K, Ghosh S K, D’Costa S L A, Naik M B, Poojary S S, Sandimani P R, Meshram G S, Jadhav R B, Bhagat S B, Gharat S M, Bakalkar C B, Prabhu T P, Anupama G C and Toomey D W 2014 *Journal of Astronomical Instrumentation* **3** 1450006 (*Preprint* 1408.4006)
- [6] Wilson J C, Hearty F R, Skrutskie M F, Majewski S R, Holtzman J A, Eisenstein D, Gunn J, Blank B, Henderson C, Smee S, Nelson M, Nidever D, Arns J, Barkhouser R, Barr J, Beland S, Bershadsky M A, Blanton M R, Brunner S, Burton A, Carey L, Carr M, Colque J P, Crane J, Damke G J, Davidson J W J, Dean J, Di Mille F, Don K W, Ebelke G, Evans M, Fitzgerald G, Gillespie B, Hall M, Harding A, Harding P, Hammond R, Hancock D, Harrison C, Hope S, Horne T, Karakla J, Lam C, Leger F, MacDonald N, Maseman P, Matsunari J, Melton S, Mitcheltree T, O’Brien T, O’Connell R W, Patten A, Richardson W, Rieke G, Rieke M, Roman-Lopes A, Schiavon R P, Sobek J S, Stolberg T, Stoll R, Tembe M, Trujillo J D, Uomoto A, Vernieri M, Walker E, Weinberg D H, Young E, Anthony-Brumfield B, Bizyaev D, Breslauer B, De Lee N, Downey J, Halverson S, Huehnerhoff J, Klaene M, Leon E, Long D, Mahadevan S, Malanushenko E, Nguyen D C, Owen R, Sánchez-Gallego J R, Sayres C, Shane N, Shectman S A, Shetrone M, Skinner D, Stauffer F and Zhao B 2019 *Publications of the Astronomical Society of the Pacific* **131** 055001 (*Preprint* 1902.00928)
- [7] Ghosh A, Sharma S, Ninan J P, Ojha D K, Bhatt B C, Kanodia S, Mahadevan S, Stefansson G, Yadav R K, Gour A S, Pandey R, Sinha T, Panwar N, Wisniewski J P, Cañas C I, Lin A S J, Roy A, Hearty F, Ramsey L, Robertson P and Schwab C 2022 *The Astrophysical Journal* **926** 68 (*Preprint* 2112.01717)
- [8] Cutri R M, Skrutskie M F, van Dyk S, Beichman C A, Carpenter J M, Chester T, Cambresy L, Evans T, Fowler J, Gizis J, Howard E, Huchra J, Jarrett T, Kopan E L, Kirkpatrick J D, Light R M, Marsh K A, McCallon H, Schneider S, Stiening R, Sykes M, Weinberg M, Wheaton W A, Wheelock S and Zacarias N 2003 *VizieR Online Data Catalog* **2246** 0
- [9] Chambers K C, Magnier E A, Metcalfe N, Flewelling H A, Huber M E, Waters C Z, Denneau L, Draper P W, Farrow D, Finkbeiner D P, Holmberg C, Koppenhoefer J, Price P A, Rest A, Saglia R P, Schlafly E F, Smartt S J, Sweeney W, Wainscoat R J, Burgett W S, Chastel S, Grav T, Heasley J N, Hodapp K W, Jedicke R, Kaiser N, Kudritzki R P, Luppino G A, Lupton R H, Monet D G, Morgan J S, Onaka P M, Shiao B, Stubbs C W, Tonry J L, White R, Bañados E, Bell E F, Bender R, Bernard E J, Boegner M, Boffi F, Botticella M T, Calamida A, Casertano S, Chen W P, Chen X, Cole S, Deacon N, Frenk C, Fitzsimmons A, Gezari S, Gibbs V, Goessl C, Goggia T, Gourgue R, Goldman B, Grant P, Grebel E K, Hambly N C, Hasinger G, Heavens A F, Heckman T M, Henderson R, Henning T, Holman M, Hopp U, Ip W H, Isani S, Jackson M, Keyes C D, Koekemoer A M, Kotak R, Le D, Liska D, Long K S, Lucey J R, Liu M, Martin N F, Masci G, McLean B, Mindel E, Misra P, Morganson E, Murphy D N A, Obaika A, Narayan G, Nieto-Santisteban M A, Norberg P, Peacock J A, Pier E A, Postman M, Primak N, Rae C, Rai A, Riess A, Riffeser A, Rix H W, Röser S, Russel R, Rutz L, Schilbach E, Schultz A S B, Scolnic D, Strolger L, Szalay A, Seitz S, Small E, Smith K W, Soderblom D R, Taylor P, Thomson R, Taylor A N, Thakar A R, Thiel J, Thilker D, Unger D, Urata Y, Valenti J, Wagner J, Walder T, Walter F, Watters S P, Werner S, Wood-Vasey W M and Wyse R 2016 *arXiv e-prints* arXiv:1612.05560 (*Preprint* 1612.05560)
- [10] Cohen M, Wheaton W A and Megeath S T 2003 *The Astronomical Journal* **126** 1090–1096 (*Preprint* astro-ph/0304350)